NIH-PA Author Manuscript

NIH-PA Author Manuscript

NIH-PA Author Manuscript

Griffonia simplicifolia Isolectin B4 Identifies a Specific Subpopulation of Angiogenic Blood Vessels Following Contusive Spinal Cord Injury in the Adult Mouse

RICHARD L. BENTON[1,3], **MELISSA A. MADDIE**[1,2], **DANIELLE R. MINNILLO**[1,4], **THEO HAGG**[1,2,5], and **SCOTT R. WHITTEMORE**[1,3,*]

[1]Kentucky Spinal Cord Injury Research Center, University of Louisville School of Medicine, Louisville, Kentucky 40292

[2]Department of Neurological Surgery, University of Louisville School of Medicine, Louisville, Kentucky 40292

[3]Department of Anatomical Sciences and Neurobiology, University of Louisville School of Medicine, Louisville, Kentucky 40292

[4]Summer Research Scholar's Program, University of Louisville School of Medicine, Louisville, Kentucky 40292

[5]Department of Pharmacology and Toxicology, University of Louisville School of Medicine, Louisville, Kentucky 40292

Abstract

After traumatic spinal cord injury (SCI), disruption and plasticity of the microvasculature within injured spinal tissue contribute to the pathological cascades associated with the evolution of both primary and secondary injury. Conversely, preserved vascular function most likely results in tissue sparing and subsequent functional recovery. It has been difficult to identify subclasses of damaged or regenerating blood vessels at the cellular level. Here, adult mice received a single intravenous injection of the *Griffonia simplicifolia* isolectin B4 (IB4) at 1–28 days following a moderate thoracic (T9) contusion. Vascular binding of IB4 was maximally observed 7 days following injury, a time associated with multiple pathologic aspects of the intrinsic adaptive angiogenesis, with numbers of IB4 vascular profiles decreasing by 21 days postinjury. Quantitative assessment of IB4 binding shows that it occurs within the evolving lesion epicenter, with affected vessels expressing a temporally specific dysfunctional tight junctional phenotype as assessed by occludin, claudin-5, and ZO-1 immunoreactivities. Taken together, these results demonstrate that intravascular lectin delivery following SCI is a useful approach not only for observing the functional status of neovascular formation but also for definitively identifying specific subpopulations of reactive spinal microvascular elements.

Keywords

neovascularization; lectin; microvascular; endothelial; tight junction; adaptive angiogenesis

*Correspondence to: Scott R. Whittemore, Kentucky Spinal Cord Research Center, 511 South Floyd Street, MDR 616, Louisville, KY 40292. swhittemore@louisville.edu.

Traumatic spinal cord injury (SCI) results in physical and molecular disruption of the delicate capillary networks within the highly vascularized spinal cord tissue. Temporally, these insults result in subarachnoid hemorrhage, inflammation, and disturbance of the blood—spinal cord barrier (BSCB). The central hemorrhage occupies the gray matter and a variable proportion of adjacent white matter at the epicenter of the injury (Noble and Wrathall, 1985). Disruption of neural and vascular structures, apparent immediately following contusion and defined as primary injury, is followed by a natural evolution of secondary pathology, which determines the extent of functional recovery (Mautes et al., 2000). Previous studies in both rats (Loy et al., 2002; Casella et al., 2002) and mice (Whetstone et al., 2003) have determined that an angiogenic response to SCI occurs within the first week postinjury and diminishes concurrently with the onset of significant histopathology and pathophysiology. Elucidation of the anatomical and functional characteristics of neovascular structures in the injured spinal cord, as well as the identification of the molecular factors responsible for vascular dysfunction following SCI, is a critical step in the development of vascularly targeted therapies. Currently no methods exist to identify neovascular/activated vessels reliably in the injured spinal cord, either at the tissue or at the cellular level.

Lectins are specific carbohydrate-binding proteins of nonimmune origin and have been used to characterize the glycosylation status specifically in a variety of tissues (Balding and Gold, 1975; Brabec et al., 1980; Franz et al., 2006). Among the larger family of lectins, two in particular have been shown to be useful for analysis of microvascular structure and function. The *Lycopersicon esculentum* (tomato) agglutinin (LEA) lectin exhibits specificity for N-acetyl-D-glucosamine-β(1,4)N-acetyl-D-glucosamine oligomers and, when delivered intravascularly, has been used widely to identify perfused microvessels in various tissues (Thurston et al., 1996; Jilani et al., 2003). In contrast, the *Griffonia simplicifolia* (Bandeiraea) isolectin B4 (IB4) specifically binds terminal α-galactosyl residues expressed by various cells including, but not limited to, endothelial cells (Peters and Goldstein, 1979; Brabec et al., 1980; Laitinen, 1987; Franz et al., 2006) in normal mouse, rabbit, rat, and human tissues (Hayes and Goldstein, 1974). More recently, intravital application of IB4 has been used to identify neovascular structures specifically within tumor vascular networks (Niethammer et al., 2002).

Increased BSCB permeability coincident with exposure to inflammatory cells is likely attributed, in part, to formation of intercellular gaps present in microvascular endothelium. This is in light of comparable observations in peripheral microvascular beds in areas of active inflammation (Thurston et al., 1996). Results from previous studies suggest that, after SCI, exposed surface membrane glycoproteins may play an important role in selective permeability of the BSCB (Noble et al., 1996). Identification of molecular changes in vascular endothelium associated with altered permeability might illuminate novel therapeutic targets to reduce secondary damage and/or improve vascular function following SCI. Markedly diminished progression of endogenous revascularization has been observed by approximately 1 week postinjury. This observation has attracted attention to the 3–7-day interval as a time frame that might best facilitate tissue sparing and regenerative therapies targeting angiogenic or antiangiogenic processes (Loy et al., 2002). Thus, the purpose of this study was twofold. First, we sought to determine whether IB4 preferentially binds vessels within the injured spinal cord actively involved in the adaptive angiogenic response and, if so, describe the temporal and spatial profile of their occurrence as well as provide initial characterization of their anatomical and functional properties. Second, we aimed to combine immunohistochemical detection of vascular epitopes (e.g., PECAM-1 and laminin) with the unique luminal glycocalyx-binding properties of lectins to visualize the functional state of microvessels within the evolving epicenter of the SCI. Together, these aims should facilitate a better understanding of the temporal and spatial nature of not only the adaptive angiogenesis but also the perfusion status of newly formed microvessels.

MATERIALS AND METHODS SCI

All surgical intervention and subsequent care and treatment of all animals used in this study were in strict accordance with the PHS Policy on Humane Care and Use of Laboratory Animals (Institute of Laboratory Animal Resources, National Research Council, 1996) and University of Louisville IACUC guidelines. In total, 48 adult female C57Bl/6 mice (18–20 g; Harlan) were anesthetized with a 1.2% avertin solution (2,2,2-tribromoethanol) given at 240 mg/kg i.p. and prepared as previously described (Papaioannou and Fox, 1993). Once anesthesia was achieved, the surgical site was prepared by shaving, and a betadine scrub and laminectomies were performed at the T7/8 vertebral level, exposing the T9/10 spinal cord segment. Without opening of the dura, mice received a moderate contusive SCI (50 kdyn force/500–600 μm displacement) using the IH impactor (Infinite Horizons Inc., Lexington, KY). The incision sites were then closed in layers, and a topical antibiotic (Bacitracin) was applied to the incision site. Animals received prophylactic injections of gentamycin to prevent infection (1 mg/kg, i.m.) and a 2-cc bolus s.c. injection of saline was given to prevent perioperative dehydration. Mice were housed five per cage, and cages were placed on a 37°C heating pad overnight. In addition, immediately following surgery and for 72 hours postoperatively, animals also received twice-daily injections of buprenorphine (Bupronex; 0.075 mg/kg i.m., b.i.d.), and their bladders were manually expressed twice daily until onset of reflexive voiding (10–14 d.p.o.).

Systemic intravascular lectin and tracer injections

At 0, 1, 3, 7, 14, 21, or 28 days post-SCI, animals were deeply anesthetized, and either 100 μg/100 μl of FITC-conjugated *Griffonia simplicifolia* isolectin B4 (IB4; Sigma, St, Louis, MO; n = 4/time point) or 100 μg/100 μl of FITC- or TRITC-conjugated *Lycopersicon esculentum* agglutinin lectin (LEA; Sigma; n = 3/time point) was delivered systemically by intravenous injection into the surgically exposed right external jugular vein and allowed to circulate for 15 minutes prior to perfusion. To assess microvascular permeability, 7 days following SCI, mice received an intravenous injection of a 2% solution Evans blue dye (EB; Sigma) 60 minutes prior to paraformaldehyde (PFA) perfusion.

Tissue processing and immunohistochemistry

After intravital infusion of IB4, LEA, or EB, mice were either transcardially perfused with saline alone (for occludin, claudin-5, ZO-1, and NG2 immunohistochemistry) or followed by 15 ml of 4% PFA, pH 7.4, for all other tissue analyses. Spinal cords were dissected and longitudinally sectioned at 20 μm on a cryostat. Sections were thaw mounted on microscope slides and stored at −80°C. On the day of staining, slides were warmed at 37°C for 20 minutes, and the mounting matrix was removed with forceps. Spinal cord tissue that was not fixed with PFA was then postfixed in ice-cold methanol for 10 minutes. Tissue was then blocked in 0.1 M Tris-buffered saline (TBS), pH 7.4, 0.1% Triton X-100, 0.5% bovine serum albumin (BSA), and 10% normal donkey serum for 1 hour at room temperature. All antibodies used in this study were obtained from commercial sources. Astrocytes were identified by using a rabbit polyclonal anti-GFAP antibody [Z0334; 1:500 dilution; immunogen: purified glial fibrillary acidic protein (GFAP) isolated from cow spinal cord; immunohistochemical (IHC) specificity: stains cells of classic astroglial morphology in the intact and injured mouse spinal cord (Jakovcevski et al., 2007); Dako, Carpinteria, CA]. Pericytes were identified by using a rabbit polyclonal antidesmin antibody [AB907; 1:50 dilution; immunogen: purified desmin protein isolated from chicken gizzard; IHC specificity: specifically stains pericytes in the adult mouse CNS (Kokovay et al., 2006); Chemicon, Temecula, CA]. Activated microglia/macrophages were visualized by using a rabbit polyclonal antiionized calcium binding adaptor molecule 1 [Iba1; 019-19741; lot HNM3505; 1:250 dilution; immunogen: synthetic peptide corresponding to amino acids 118–131 within the c-terminus of Iba1; IHC specificity: stains ramified microglia within the adult mouse CNS (Hirasawa et al., 2005); Wako, Richmond, VA].

Activated endothelium-associated pericytes were visualized by using a polyclonal rabbit anti-NG2 antibody [AB5320; 1:50 dilution; immunogen: purified NG2 chondroitin sulfate proteoglycan isolated from rat; IHC specificity: stains pericytes in activated mouse tumor endothelium (Sennino et al., 2007); Chemicon]. Proliferating cells were identified by using a polyclonal rabbit anti-Ki67 antibody [NCL-Ki67p; 1:500 dilution; immunogen: purified prokaryotic recombinant Ki67 protein; IHC specificity: recognizes proliferating cells (including endothelial cells) in the adult mouse (Edsbagge et al., 2005); Novocastra Laboratories, Newcastle upon Tyne, United Kingdom]. Apoptotic/ necrotic cells were identified by using a polyclonal rabbit antiapoptosis-inducing factor [AIF; AB16501; 1:100 dilution; immunogen: a peptide corresponding to amino acids 517–531 of human AIF; IHC specificity: stains apoptotic/necrotic cells in the adult mouse spinal cord (Chi et al., 2007); Chemicon] or the Apoptag in situ apoptosis detection kit (S1100; Chemicon) used according to the manufacturer's protocol.

The presence and functional status of spinal microvessels were also assessed in this study by using immunohistochemistry. Vascular endothelial cells were identified with a monoclonal rat anti-PECAM-1 antibody [550274; clone MEC13.3; 1:50 dilution; immunogen: cell membrane fractions from mouse derived endothelioma cell line tEnd.1; IHC specificity: labels vascular endothelium in the adult mouse spinal cord (Hsu et al., 2006); BD Pharmingen, San Diego, CA]. The integrity of the vascular endothelial basal lamina matrix was examined by using polyclonal rabbit antilaminin [L9393; 1:100 dilution; immunogen: purified laminin from basement membrane of EHS mouse sarcoma; IHC specificity: basal lamina of spinal vascular endothelium (Loy et al., 2002); Sigma] and/or polyclonal rabbit anticollagen type IV [T40263R; 1:100 dilution; immunogen: purified mouse type IV collagen; IHC specificity: stains basal lamina of existing and angiogenic vessels in rodent spinal cord (Loy et al., 2002); Biodesign International, Saco, ME). Clotting-competent vascular endothelial cells were examined by using a polyclonal rabbit anti-von Willebrand factor/factor VIII (vWF) antibody [A0082; 1:200 dilution; immunogen: vWF purified from human plasma; IHC specificity: stains vascular endothelial cells in the mouse CNS (Alliot et al., 1999); Dako, Capinteria, CA]. The metabolic potential of vascular endothelial cells was assessed by using a polyclonal rabbit antiglucose transporter type 1 (Glut-1) antibody [AB1340; 1:100 dilution; immunogen: a synthetic peptide corresponding to amino acids 332–343 within the c-terminus of rat Glut-1; IHC specificity: stains spinal vascular endothelial cells in the intact/injured mouse spinal cord (Whetstone et al., 2003); Chemicon]. The molecular integrity of the BSCB was examined by using polyclonal rabbit antioccludin [clone Z-T22; 1:50 dilution; immunogen: a synthetic peptide corresponding to amino acids 372–522 of the c-terminus of human occludin; IHC specificity: stains vascular endothelial cells from the adult mouse spinal cord (Ge and Pachter, 2006)], polyclonal rabbit anti-ZO-1 [clone ZR1; 1:50 dilution; immunogen: fusion protein corresponding to amino acids 463–1109 of human ZO-1; IHC specificity: stains vascular endothelial cells in the adult mouse CNS (Stamatovic et al., 2005)], and polyclonal rabbit anticlaudin-5 [clone Z43.JK; 1:50 dilution; immunogen: synthetic peptide derived from amino acids 150–218 of the c-terminal sequence of mouse claudin-5; IHC specificity: specifically stains endothelial cells in the adult mouse CNS (Nitta et al., 2003)], all from Zymed (Carlsbad, CA). All positive staining observed in the spinal cord for each antibody used is consistent with previous reports. Negative control for each antibody staining was accomplished by the parallel substitution of species-matched preimmune IgG, which resulted in no staining. Primary antibodies were applied in 0.1 M TBS, pH 7.4, 0.1% Triton X-100, 0.5% BSA, and 5% normal donkey serum overnight in a humidified chamber at 4°C. Sections were then incubated with rhodamine (TRITC; 1:200)- or AMCA (1:100)-conjugated secondary antibodies (Jackson Immunoresearch, West Grove, PA) for 1 hour at room temperature in a humidified chamber. Sections were then washed for 3×10 minutes at room temperature in 0.1 M TBS, pH 7.4. All photomicrographs demonstrating immunostained spinal cord sections were captured with a Nikon TE 300 inverted microscope equipped with a Spot CCD camera and Metamorph capture

software (Diagnostic Instruments, Sterling Heights, MI), an LS-500 laser confocal microscope (Olympus Inc., Center Valley, PA), or an Eclipse C1 laser confocal microscope (Nikon Instruments Inc., Melville, NY). The brightness and color balance of photomicrographs used for illustration were adjusted for qualitative consistency in Adobe Photoshop CS2 (version 9.0.2; Adobe Systems Inc., San Jose, CA). All figures were assembled in Adobe Illustrator CS2 (version 12.0; Adobe Systems Inc.).

Quantitative assessment of spinal microvascular density and intravascular lectin binding

Quantitative assessment of intravascular lectin binding and vascular endothelial immunohistochemistry was accomplished by using methods similar to those previously described (Loy et al., 2002) with Image Pro Plus software (Media Cybernetics, Silver Spring, MD). To minimize variability in immunostaining, all replicates (n = 3 or 4/experimental group) were processed for PECAM-1 immunohistochemistry simultaneously. Furthermore, to minimize variability in photomicroscopic images used for quantitative assessment, images were acquired using identical exposure settings for each analytical group (PECAM-1 ihc, FITC-IB4 and FITC-LEA binding). Images of every fifth longitudinal section through the entire dorsoventral axis of the spinal cord from each experimental case were captured and imported into the analysis software. In spinal cord tissue taken from mice 7 and 14 days post-SCI, the injury epicenter was defined as the domain exhibiting significant extravascular laminin deposition (see Fig. 2D,E; hatched outlines). At earlier time points (1 and 3 days post-SCI), the evolving epicenter was defined as the area exhibiting disorganization of vascular laminin immunoreactivity (see Fig. 2B,C; hatched outlines). The injury epicenters were then manually traced for each section (20–25 sections/experimental replicate) and automatically converted to an area of interest (AOI) by the software. The area of each AOI was then automatically calculated by the software and exported to an Excel (Microsoft Corp., Redmond, WA) spreadsheet. For analysis of sham-injured control tissue, an AOI mask representing the mean area of all experimental AOIs was applied to each control section and served as the defined area for analysis of baseline immunostaining/binding. Once this was defined, the contrast, brightness, color balance, and contrast were adjusted to identical settings for each AOI. After normalization of brightness and contrast, the total number of pixels of binding/staining above threshold was then automatically calculated for each AOI. The per area density of binding/ staining for each image was then calculated by dividing the total pixels of binding/staining by the AOI area in pixels. For each experimental case, the total per area density of binding/staining was obtained by summing (approximately 20–25 sections total/experimental case) the values obtained for each section analyzed, which represented an approximate spatial resolution of 100 μm throughout the entire dorsoventral axis of each spinal cord. Statistical analysis of all these data was accomplished via one-way ANOVA with a Tukey HSD post hoc *t*-test.

Immunoelectron microscopy

At 7 days following SCI, one group of additional mice (n = 3) was deeply anesthetized and intravitally infused with 100 μg FITC-conjugated IB4. Fifteen minutes later, mice were perfused with 2% PFA/2.5% glutaraldehyde, pH 7.4. Spinal cords were dissected, and the injury epicenters were sectioned transversely at 30 μm with a microtome. Sections were incubated overnight with a biotinylated rabbit anti-FITC antibody (1:100), followed by 3,3-diaminobenzidine detection via Vectastain Elite kit (Vector, Burlingame, CA). Sections were postfixed in osmium tetroxide, dehydrated, and embedded in Embed-812. Ultrathin sections were analyzed and photographed with a Philips CM10 transmission electron microscope.

RESULTS

Spinal microvascular anatomy and function are altered in the injured murine spinal cord

By concurrent examination of spinal microvascular basal lamina (laminin; AMCA), microvascular endothelium (PECAM; TRITC), and perfusion state (LEA; FITC) the temporal, spatial, and functional courses of the SCI-induced vascular changes are apparent (Fig. 1). In spinal cord tissue from sham-operated mice (Fig. 1A,B), a dense vascular network is apparent, with microvessels demonstrating an intact basal lamina, prominent endothelium, and definitive perfusion of intravascular LEA labeling. Consistent with previous reports (Loy et al., 2002; Casella et al., 2002,2006;Whetstone et al., 2003), 24 hours after experimental SCI, markers for vascularity are diminished at the injury epicenter, which then partially reappear within the first 7 days post-SCI (Fig. 1C—H), which is suggestive of angiogenesis. By using intravascular tracing techniques, we observed a paucity of perfused microvessels at the injury site at 24 hours following SCI, concomitant with the appearance of a vascular phenotype possessing a basal lamina but devoid of PECAM-1-ir, a marker of vascular endothelial cells (Fig. 1C,D). At 3 days post-SCI, spinal endothelium coincident with vascular laminin immunostaining is apparent as well as the reappearance of LEA luminal binding in these vessels (Fig. 1E,F), which was also observed through day 7 post-SCI (Fig. 1G,H). By 14 days post-SCI, a dense revascularization is observed within the injury epicenter, with many of the vascular profiles also containing luminal LEA binding (Fig. 1I,J), which is suggestive of a restoration of the perfusion state within newly formed vascular networks.

Temporal and spatial analysis of IB4 vascular binding after intravital infusion following SCI

Quantitative analyses of luminal binding of IB4 relative to total vascular endothelial cell content (i.e., PECAM-1-immunoreactive density) in the injury epicenter (see Fig. 3) showed that, as early as 1 day post-SCI, activated vessels are present within the injury epicenter. The presence of IB4-bound vessels gradually increased, reaching maximal levels by 7 days postinjury. This increase in IB4-bound vessels at the injury epicenter coincides with the formation of the area rich in extravascular laminin and pathological matrix species (Figs. 2A—D), which is characteristic of the evolving injury in the contused mouse spinal cord. At 28 days post-SCI, which represents the latest time point evaluated, the degree of luminal IB4 binding approached control levels but was still significantly higher than that in naïve thoracic spinal tissue. Approximately 86% of all observed IB4 vascular phenotypes are located within the injury epicenter (data not shown), which is readily observed as the stabilized scar matrix observed beyond 7 days postinjury at the contusion epicenter (Fig. 2D—G).

Combinatorial IHC and intravascular labeling demonstrates differential microvascular phenotypes temporally in the injury epicenter

Consistent with previous findings in the mouse (Whetstone et al., 2003) and rat (Loy et al., 2002), we observed a precipitous decrease in PECAM-1-immunopositive endothelium within the injury epicenter by 1 day following SCI (Fig. 3A). Endothelium detected within the injury epicenter gradually increased during the first week following injury, with a reappearance of PECAM-1 immunopositive vascular profiles reaching 70% of control values by 14 days postcontusion, which is consistent with an adaptive angiogenic response. When the temporal appearance of intraluminal LEA, which has been used as a marker of microvascular perfusion in the murine spinal cord (Yamauchi et al., 2004), is plotted against the increase in PECAM-1 immunostaining, a temporal lag in perfusion of these vessels is apparent. In control spinal tissue, all vessels within thoracic spinal tissue exhibit luminal LEA binding (Figs. 1A,B, 3B). One day following injury, vascular LEA binding is significantly reduced, coincident with the regression of injured microvessels immediately following SCI. Vascular LEA binding begins to recover within the injury epicenter by 3 days postinjury, with levels of luminal LEA binding increasing to approximately 20% of those observed in control tissue. This is a significant

finding compared with the >50% recovery of control levels observed for PECAM-1-ir. It is not until 14 days postinjury when the intraluminal binding of LEA is significantly higher than that observed 24 hours following SCI. Additionally, the temporal appearance of vessels within the injury epicenter binding the IB4 lectin corresponds to this dynamic phase of adaptive angiogenesis (Fig. 3C). It is important to note that maximal binding of IB4 occurs at 7 days post-SCI, which immediately precedes the significant increase in LEA binding in affected microvessels, suggesting that the IB4 phenotype represents a transitory, neovascular structure. Taken together, these results suggest that newly formed blood vessels in the SCI epicenter are not fully functional, exhibiting a delay in their reestablishment of perfusion.

IB4-bound microvessels also demonstrate intraluminal LEA binding

In a subset of mice (n = 3), both LEA (TRITC-conjugated) and IB4 (FITC-conjugated) were delivered intravascularly 7 days following injury. This was done to assess the specific glycoconjugate phenotype associated with angiogenic microvessels in the injury epicenter as well as to determine the validity of LEA as a marker of spinal microvascular perfusion. Qualitative results indicated that IB4-bound vessels in the injury epicenter also exhibit luminal LEA binding (Fig. 4). This finding suggests that perfused vessels within the injury epicenter retain the capacity for luminal LEA binding, irrespective of their state of activation. This result validates the conclusion that the IB4 phenotype represents a unique subpopulation of activated spinal cord vessels and demonstrates the utility of intravital LEA administration as a measure of spinal cord microvascular perfusion following SCI.

Ultrastructural analysis of IB4-bound spinal microvessels demonstrates an intact endothelium with variable degrees of abluminal histopathology

To characterize better the histopathology associated with the IB4 microvascular phenotype, immunoelectron microscopy was performed on spinal cord tissue taken from mice receiving intravascular IB4 7 days following injury. In sham spinal cords (Fig. 5A,B), no luminal IB4 binding was observed. Furthermore, normal microvascular ultrastructure is apparent (Fig. 5C), with capillaries surrounded by an intact abluminal matrix and normal pericytic investment. By contrast, spinal cord sections taken from SCI mice grossly exhibited robust binding of IB4 (Fig. 5D,E), especially within the capillary bed of the affected spinal gray matter. Ultrastructural assessment demonstrated microvessels not binding IB4 in close proximity to those expressing the pathologic luminal phenotype (Fig. 5F), suggesting that the IB4 phenotype is expressed only within a subset of vessels in the injured area. One consistent finding from the ultrastructural assessment is significant extravascular matrix disruption (Fig. 5F—I) as well as the presence of perivascular inflammatory cells (Fig. 5G). Ultrastructural analyses demonstrate an intact endothelium in microvessels binding IB4 (Fig. 5G—I).

Significant histopathology is observed concomitant with intravascular IB4 binding

To evaluate possible pathologic cellular—endothelial interactions, which may be related to the onset of the microvascular IB4 phenotype following SCI, the distributions of both cellular and acellular elements known to be associated with microvascular stabilization were assessed. In the uninjured mouse spinal cord, a dense astroglial investment of capillaries is apparent (Fig. 6A), which demonstrates the presence of astroglial perivascular networks known to contribute to the normal, intact blood—CNS barrier (for review see Abbott et al., 2006). Consistent with previous reports (Fujiki et al., 1996;Ma et al., 2001;Whetstone et al., 2003), an area devoid of astrocytes was observed at the contusion epicenter 7 days post-SCI (Fig. 6B). The IB4 microvascular phenotype largely colocalized to areas devoid of astrocytes following injury, with only a few IB4-bound vessels present at the marginal zone of the astrocyte-free domain (Fig. 6C). Perivascular desmin immunostaining in control spinal tissue, which has been interpreted as an indicator of pericyte-mediated microvascular stability in the CNS (Hughes et

al., 2006), demonstrates punctate desmin immunoreactivity enriched at vascular branch points consistent with pericyte investment of spinal microvessels (Fig. 6D). At 7 days following SCI, desmin immunoreactivity is largely absent from IB4-bound microvessels (Fig. 6E,F), suggesting a loss of pericyte ensheathment of the affected microvessels. This observation was confirmed by ultrastructural evaluation (Fig. 5F—I). Also, association of the IB4 vascular phenotype with robust immunostaining for Iba1, which is a marker of activated microglia/macrophages, demonstrates that the IB4 phenotype is localized to areas of active inflammation in the injured spinal cord (Fig. 6H,I). By 7 days following SCI, IB4-bound microvessels demonstrate associated collagen IV immunoreactivity within the evolving lesion epicenter (Fig. 6K,L), suggesting a partial preservation of a nonpathological basal lamina component, which is suggestive of partial preservation in abluminal integrity.

Spinal microvessels binding IB4 demonstrate dysfunctional phenotypes

To assess the functional phenotype of the subpopulation of spinal microvessels binding IB4 following SCI, we examined the expression of several markers of spinal microvascular function in the affected microvasculature. In the intact CNS, expression of the chondroitin sulfate proteoglycan NG2 is observed mainly in mural cells of the microvasculature but, in response to injury, is highly expressed in several activated cellular compartments, including activated microvascular endothelial cells (for review see Morgenstern et al., 2002). In control spinal cord tissue, NG2 immunoreactivity is seen as sparse, discontinuous/punctate signal associated with microvessels (Fig. 7A), a pattern that is consistent with moderate levels of expression in the mural cellular compartment. Seven days following SCI, NG2 expression is readily observed as robust immunoreactivity associated with IB4-bound microvessels (Fig. 7B,C), suggesting a general state of cellular activation. We also observed significant extravasation of EB associated with IB4-bound vessels in the injury epicenter (Fig. 7J,K), demonstrating that this subpopulation exhibits characteristics of macromolecular hyperpermeability. Additionally, expression of the type 1 glucose transporter (Glut-1), which is expressed exclusively by vessels in the uninjured mouse spinal cord (Fig. 7D), is absent from IB4-bound microvascular profiles (Fig. 7E,F). This observation is consistent with previous reports of diminished endothelial expression of Glut-1 in spinal microvascular endothelial cells following traumatic SCI (Whetstone et al., 2003). Endothelial overexpression of the prothrombotic protein von Willebrand factor (vWF) is associated with endothelial disease and dysfunction, especially within the endothelium of the cardiovascular system proper (Vischer, 2006). To date, it is unknown what contribution vWF expression within the injured spinal microvasculature makes to the onset of pathologic platelet aggregation as it relates to microthrombosis following experimental SCI. In uninjured spinal microvessels, low basal expression of vWF is observed associated with LEA-bound vascular profiles (Fig. 7G). Seven days following injury, robust expression of vWF colocalizes to a subset of IB4-bound spinal microvessels (Fig. 7H,I). This finding is suggestive of a role for vWF-mediated microthrombosis as a complicating factor in the posttraumatic reperfusion of affected intrinsic spinal microvessels.

IB4-bound spinal microvessels represent a proliferative neovascular endothelial subpopulation in the injured spinal cord

To determine whether the IB4 vascular phenotype represents a regressive or proliferative vascular phenotype, we examined spinal cord sections for IB4 colocalization with various markers of cellular activation status. Although many IB4-associated endothelial cells were found to be TUNEL negative (Fig. 8A,D, single-tipped arrows), small numbers of IB4-associated endothelial cell nuclei appeared to be TUNEL positive (Fig. 8B,C, double-tipped arrows). However, these nuclei did not exhibit nuclear condensation or fragmentation characteristic of apoptotic cells, as did other nonendothelial cell nuclei in the fields examined (Fig. 8A—D, arrowheads). This suggests that IB4-positive endothelial cells do not undergo "classical" apoptosis. Furthermore, no IB4-labeled vascular profiles were observed expressing

apoptosis-inducing factor (AIF; Figs. 8E—H). In contrast, many nonvascular cells express AIF within the SCI epicenter in both its nonactivated (perinuclear; Fig. 8E) and its activated (nuclear; Fig. 8G) forms. Comparatively, we observed a number of endothelial nuclei associated with IB4-bound microvessels that were positive for the cell proliferation marker Ki67 (Fig. 8I—L, arrows). Taken together, these results suggest that the IB4 vascular phenotype represents a largely proliferative subpopulation of microvessels within the area of active adaptive angiogenesis in the injury epicenter.

A specific temporal course of pathological endothelial tight junctions is associated with the appearance of the IB4 vascular phenotype

Interendothelial junctions within the normal endothelium of the nervous system consist of several junctional complexes and include both transmembrane and intracellular components. These endothelial specializations contribute to normal vascular function as well as contributing to the tightly regulated barrier function characteristic of CNS vasculature (Bazzoni and Dejana, 2004). Specifically, we examined the dynamics of spinal microvascular tight junction (TJ) complexes in the evolving injury epicenter by performing immunohistochemical detection of the transmembrane proteins occludin and claudin-5 as well as the intracellular TJ component ZO-1. In control spinal tissue, endothelial cells of quiescent microvasculature demonstrate robust expression of the TJ proteins occludin, claudin-5, and ZO-1 (Fig. 9A—C). At 1 day post-SCI, the spared vessels within the injury epicenter express grossly normal distributions of these TJ components (Fig. 9D—F) compared with control. Three days following SCI, which coincides with the initial appearance of significant numbers of IB4-bound vessels, pathological expression of TJ subunits is apparent. At this time point, the majority of IB4-bound vessels express normal distribution of both claudin-5 (Fig. 9H) and ZO-1 (Fig. 9I). In contrast, IB4 vascular profiles appear to express both abnormal distribution and low levels of occludin (Fig. 9G) relative to nonpathologic vascular profiles. By 7 days following SCI, IB4-bound vessels express overt signs of TJ pathology characterized by total loss of occludin expression (Fig. 9J) and a dramatic alteration in both levels and distribution of claudin-5 immunostaining (Fig. 9K). Immunostaining for the intercellular TJ component ZO-1 was present in IB4 vascular profiles (Fig. 9L), although the appearance of the immunostaining was markedly altered with respect to both its distribution and its continuity along the vascular profile. At 14 days post-SCI, which represents the latest postinjury time point when significant numbers of IB4-bound vessels are observed, all TJ components are absent from affected vessels. Taken together, these results are the initial documentation of TJ pathology commensurate with spinal microvascular plasticity and dysfunction following experimental SCI.

DISCUSSION

Combinatorial intravital and immunohistochemical approaches better demonstrate the temporal revascularization and reperfusion of vessels in the injured spinal cord

After SCI, the loss of spinal microvascular endothelial cells, by both necrotic and apoptotic cell death, is rapid, with significant decreases in cell numbers observed as early as 15 minutes post-SCI (Casella et al., 2006). In the subchronic phase of the injury, an endogenous adaptive angiogenesis occurs in both rats (Loy et al., 2002; Casella et al., 2002) and mice (Whetstone et al., 2003), which has been characterized by a revascularization of the injury epicenter as evidenced by immunohistochemical detection of microvascular elements (i.e., PECAM-1, RECA-1, laminin, and collagen IV). These previous studies failed to address the functional/perfusion status of the epicenter and penumbral microvasculature as the injury evolved. This is an important issue in light of previous data from Tator and colleagues illustrating a significant lack of perfusion in "immunohistochemically intact" spinal capillary beds following injury (Koyanagi et al., 1993). Furthermore, recent observations in studies of experimental peripheral tumor angiogenesis demonstrate a disconnection between microvascular anatomy in

angiogenic foci and perfusion of those affected vascular beds (Noguera-Troise et al., 2006). Thus, the impetus for the current study is based on these findings and the possibility that the immunohistochemical detection of microvascular elements within the spinal cord might not be evidence of a functional microvascular network.

LEA has been used extensively as a histochemical reagent to identify various anatomical features within the CNS, including endothelial cells (Mazzetti et al., 2004). More relevant to the current study is the finding that intravascular LEA administration may be an effective anatomical marker of spinal perfusion following trauma (Yamauchi et al., 2004). We apply this methodology along with traditional immunohistochemical techniques to identify microvascular elements within the injured spinal cord that lack apparent perfusion (Fig. 1). This is an important finding in light of the fact that quantification of PECAM-1 (Glaser et al., 2004) as well as the endothelial surface antigen RECA-1 (Richter et al., 2005) have been used as independent measures to evaluate the efficacy of therapeutic interventions on vascular stability and/or promotion of angiogenesis following SCI. Although these approaches are certainly valid for identifying vascular networks, their use as markers of vascular function may not be optimal to evaluate therapeutic alteration of spinal microvascular function following SCI. The current results add to the understanding of the potential functional state of the newly formed vasculature within the injury epicenter, but they are by no means a definitive demonstration of the functional state of the microvasculature at the site of injury. Thus, future experiments demonstrating a correlation between anatomical perfusion and functional in vivo perfusion status (e.g., via microlaser Dopler flowmetry and/or oximetry) should provide irrefutable evidence of the temporal lag of regeneration and reperfusion of neovascular elements in the injured spinal cord.

Intravital application of IB4 identifies a specific subpopulation of spinal microvessels within the evolving injury epicenter

The surface glycoconjugate phenotype for endothelium from various organs appears to be somewhat the same, with independent lectin types binding endothelium from different tissues with apparent specificity (Belloni and Nicolson, 1988). In various extra-CNS experimental paradigms, intravital IB4 has been used to examine endothelial plasticity during development (Jilani et al., 2003), chronic inflammation (Thurston et al., 1996), and tumor neovascularization (Debbage et al., 1998).

In the immature CNS, a specific transformation toward an overall negatively charged luminal glycocalyx has been observed with the histochemical application of various lectins (Vorbrodt et al., 1986). This is an important observation insofar as the phenotype of the CNS vascular glycocalyx plays a central role in vascular function and blood—brain barrier integrity (Nico et al., 1998). Pertubation of the luminal glycocalycal phenotype results in pathologic changes in permeability (Vorbrodt, 1986) and significant neuroinflammation (Nico et al., 2000). Others have utilized the histochemical application of various lectins to demonstrate pathologic microvascular structure following stroke (Nishida et al., 1986) or traumatic SCI (Noble et al., 1996). Intravital lectin delivery has been used less frequently, although it has been employed to characterize histopathologic transformation in cortical CNS microvessels following experimental stroke (Nishida et al., 1986) and hypertension (Nag, 1984).

IB4 has been widely used as a histochemical reagent on tissue sections to label glycoconjugates specifically on various CNS cell types, including neurons, glia, and activated microglia (Streit et al., 1985; Morioka et al., 1993). Furthermore, it is known to identify vessels in the normal (Fatehi et al., 1987), developing (Hughes and Chang-Ling, 2000; Vinores et al., 2003), and diseased (Chan-Ling et al., 2004) CNS. Although the latter studies demonstrate neovascular structures within complex microanatomy, intravital application of IB4 allows for much clearer resolution of neovascular profiles within the injury epicenter. Consistent with applications

identified in the above-cited studies, application of IB4 to sections of injured spinal tissue primarily identifies pathologic ECM, inflammatory cells, and degraded neuropil (Fig. 2F,G). Intravascular administration of IB4 does not label microvessels exposed to inflammatory induction outside of the CNS (Thurston et al., 1996), whereas this is clearly the case in the present study. These disparate results are likely the result of heterogeneity in responses to injury/insult in these two vascular beds.

Most IB4-bound microvessels observed in this study appear to retain the capacity for LEA reactivity within the injured spinal cord (Fig. 4). This is significant in that it suggests that the lack of LEA intravascular binding in regenerating PECAM-1 vascular profiles is not the result of a lack of glycoconjugate in the luminal glycocalyx but indicates a true lack of perfusion in the affected vascular bed. Additionally, this finding highlights the transitory nature of this transformation and demonstrates that the IB4 vascular phenotype is a specific luminal marker for neovascular structures in the injured mouse spinal cord.

The IB4 vascular phenotype represents a proliferative subpopulation of spinal microvascular endothelial cells

We demonstrate sparse labeling of IB4-positive endothelial cell nuclei for TUNEL, but an absence of overt nuclear condensation. Furthermore, we did not detect translocation of cytoplasmic AIF immunoreactivity to the nuclei of IB4-bound endothelium, a characteristic of necrotic cell death. Conversely, IB4-positive endothelial cells often had Ki67-immunoreactive nuclei, which is suggestive of a proliferative population of angiogenic vessels. Relevant to this finding are results indicating that in vitro induction of late-stage apoptotic cell death results in the differential pathologic glycosylation of cell membranes, which can then be specifically detected by various nonlytic lectins, including IB4 and *Ulex europaeus* (UEA; Franz et al., 2006). In support of the conclusion that IB4 vascular profiles represent a largely proliferative subpopulation, we have performed pilot experiments with double intravascular labeling using UEA and IB4. Preliminary results from these experiments do not demonstrate IB4/UEA double-labeled microvessels in spinal cord tissue 7 days post-SCI (data not shown). It is unknown whether this is further evidence against an affinity of intravascular IB4 for dying spinal endothelial cells or merely a phenomenon associated with a species-specific glycoconjugate modification, insofar as previous results have shown a lack of UEA binding of murine endothelium (Ponder and Wilkinson, 1983; Iruela-Arispe et al., 1999).

Intravascular IB4 identifies a population of endothelial cells exhibiting abnormal TJ phenotypes in the injured murine spinal cord

Within the CNS endothelium, strict control of macromolecular passage is facilitated by the BBB, which is provided by well-developed TJ complexes (for review see Bazzoni and Dejana, 2004). Alteration of these TJ connections between adjacent endothelial cells is hall-mark of the initiation of microvascular dysfunction and is associated with multiple pathologies (Wolburg et al., 2003). For example, abnormal cellular localization and expression of TJ components are observed associated with endothelial cell stress following hypoxic insult (Mark and Davis, 2002) and a pathologic loss of endothelial cell polarity and abnormal glucose transport potential in spontaneously hypertensive rat BBB endothelial cells (Lippoldt et al., 2000). Pathologic changes in occludin, claudin-5, and ZO-1 levels and distribution are associated with the acute phase of hyperpermeability in brain microvessels (Dobrogowska and Vorbrodt, 2004). To date, no data exist supporting a similar mechanism giving rise to spinal microvascular dysfunction following SCI. This is an important issue, insofar as it stands to reason that alterations in the TJs responsible for providing tight interendothelial connection could potentiate transcellular permeability from the spinal circulation into the parenchyma. We demonstrate that TJs are pathologically altered in activated spinal microvascular endothelial cells following SCI. The temporal specificity of these changes correlates well with

the acute phase of spinal microvascular dysfinction and hyperpermeability observed following SCI (Noble and Wrathall, 1989b; Whetstone et al., 2003).

Occludin, which is thought to be the apicalmost TJ subunit in CNS endothelium (Vorbrodt and Dobrogowska, 2003), is the first component lost from affected spinal microvessels (Fig. 8G). The temporal aspect of the loss of occludin-ir in the IB4 vascular phenotype coincides with previous reports of loss of another luminal component of the BSCB, endothelial barrier antigen (EBA), following contusion of the rat spinal cord (Perdiki et al., 1998). Thus, the loss of apical interendothelial connection likely contributes to the paracellular extravasation of both cellular and acellular elements during the acute phase of secondary injury cascades following SCI. Furthermore, previous results demonstrate that the ultrastructure of spinal endothelial TJ integrity is altered following SCI, with approximately 20% of all affected microvessels exhibiting characteristic clefts within TJ complexes (Jaeger and Blight, 1997). This observation is consistent, both spatially and temporally, with the abnormal distribution of immunoreactivity for the TJ components found to be associated with IB4-bound spinal vessels. Furthermore, the temporal specificity of the interendothelial junctional alterations observed in the current study is consistent with previous findings demonstrating that occludin and ZO-1 are lost during early phases of experimental inflammatory lesion to the cortex (Bolton et al., 1998).

Also important is the observation that most of the affected spinal microvessels occur largely within areas of significant astroglial loss (Fig. 6A—C). This overt loss of astrocytes is associated with the histopathologic progression at the lesion epicenter in experimental murine SCI (Fujiki et al., 1996; Ma et al., 2001). Astrocytes are potent regulators of CNS endothelial TJ phenotype, both in vitro (Raub, 1996) and in vivo (Willis et al., 2004). In the Willis et al. study, focal loss of astrocytic investment in brain endothelial cells resulted in altered expression of occludin, ZO-1, and claudin-5, which resulted in increased permeability in affected microvessels. Alternatively, results from in vitro modeling of BBB changes correlative to TJ component dysregulation suggests that BBB/BSCB integrity may be more dependent on microvascular investment of astroglial endfeet than intact TJ complexes, in that loss of junctional components from cellular contacts did not result in significant increases in modeled permeability (Hamm et al., 2004). Although current data do not definitively imply the associated hyperpermeability associated with the IB4 vascular phenotype (Figs. 7J,K) with altered TJ pathology, the ability to identify clearly pathologic spinal microvessels using intravital IB4 may prove useful in more directly addressing this issue in future experiments.

The ability to identify spinal microvessels devoid of astroglial investment by using intravascular IB4 might have other important implications for attenuation of neuropil loss following SCI. The loss of astroglial investment is thought to result in abnormal glucose transport potential within the affected endothelium (Whetstone et al., 2003). We observed that IB4-bound microvascular elements do not demonstrate Glut-1 immunoreactivity (Fig. 7E,F). This is another indication of overt pathophysiology in the IB4 microvascular subpopulation, in that Glut-1 is critically important for the metabolic potential within the injury epicenter. This likely has important implications for tissue preservation; Glut-1-mediated glucose supply is thought to be the predominant pathway for support of parenchymal metabolism in the spinal cord (for review see McEwen and Reagan, 2004).

Experimental utility and significance of the IB4 microvascular phenotype in the injured spinal cord

Microvascular activation/dysregulation within the injured spinal cord is of paramount importance, in that it is hypothesized to underlie aspects of both acute and chronic pathologic phases following SCI. Acutely, microvascular damage results in significant hemorrhage (Noble and Wrathall, 1989a), which is directly toxic to neuropil (Bullock and Fujisawa, 1992). Chronically, microvascular dysfunction contributes to multiple secondary injury

cascades (for review see Mautes et al., 2000). One difficulty in studying microvascular responses during this later phase of injury has been the lack of definitive markers for activated endothelial cells in injured spinal tissue. One recently characterized negatively regulated marker of endothelial activation in the murine SCI model is the loss Glut-1 expression in affected microvessels during this critical phase of vascular dysfunction (Whetstone et al., 2003). We extend this result by identifying a positive phenotypic marker of this vascular subpopulation using intravital IB4, making future examination of microvascular plasticity feasible.

Another important finding is that the IB4 vascular phenotype is associated with areas of active inflammation in the injured spinal cord. Thus, it may be plausible to utilize the differential appearance of this subpopulation of vessels as an endpoint assessment of interactions of inflammatory cells with the vasculature. This could be useful insofar as several promising experimental therapies targeting the inflammatory responses following SCI are currently under development and appear to have beneficial effects (Gris et al., 2004; Bao et al., 2005; Oatway et al., 2005). Furthermore, the potential functional implication of endothelial cell upregulation of $\alpha 1,3$-galactosyltransferase, which is a major enzyme responsible for the generation of the glycoconjugates recognized by IB4, may be significant for the propagation of multiple secondary injury cascades following SCI. An important function of these glycoconjugates in vascular function is the selectin-dependent recruitment of leukocytes to sites of inflammation (Lowe, 2003). The temporally specific increase in the α/β-1,3-galactose expressed on the luminal surface of affected endothelium detected here likely contributes to the propagation of the active inflammatory processes occurring in the mouse spinal cord 3–14 days post-SCI. After experimental mouse (Kigerl et al., 2006) and rat (Popovich et al., 1997) SCI, active extravasation of inflammatory cells begins to peak by 3 days postinjury, which coincides with the initial observation of the IB4 luminal phenotype. It remains to be determined whether experimental targeting of the α/β-1,3-galactose glycoconjugate groups as a means to decrease inflammatory cell infiltration might hold therapeutic promise. Nonetheless, based on the current characterization of the microenvironment where IB4 microvascular binding is observed, this pathologic transformation likely is driven by one or more factors enriched in the inflammatory microenvironment, consistent with the known proangiogenic role of cellular inflammatory mediators (for review see Han and Suk, 2005). The direct utility of masking of these specific epitopes in controlling inflammation following experimental SCI is an intriguing possibility. Another interesting issue is the exploitation of the IB4 vascular phenotype to target therapeutics luminally to sites of vascular dysfunction in the injured spinal cord. Similar approaches have been used successfully in other CNS pathologies; it appears that they circumvent the rigid exclusion of potentially therapeutic macromolecules by the BBB/BSCB (Pardridge, 2007).

The primary issue related to the clinical relevance of the current study relates to the question of whether the specific glycoconjugate phenotype detected in the activated spinal microvasculature is unique to the mouse model. Although we have observed a comparable response in the rat spinal contusion model (data not shown), it is unknown whether a comparable response is seen in clinical cases of human SCI. It is possible that the transformation to an IB4 phenotype within affected microvessels is a phenomenon specific to the rodent experimental model, insofatr as *Griffonia simplicifolia* IB4 does not exhibit vascular binding when applied as a histochemical reagent in human vascular endothelial cells (Alroy et al., 1987). This observation is consistent with an apparent absence of the rate-limiting enzyme responsible for production of α-D-galactosyl residues on the cell surface in humans and nonhuman primates (Galili et al., 1988). The more general question is whether similar alterations of the glycocalyx occur following human SCI. To date, no report exists regarding this issue; if such changes are demonstrated they may provide better insight into potential

mechanisms underlying vascular dysfunction following human SCI as well as identify novel targets for potential therapeutic intervention.

ACKNOWLEDGMENTS

LITERATURE CITED

Abbott NJ, Ronnback L, Hansson E. Astrocyte—endothelial interactions at the blood—brain barrier. Nat Rev Neurosci 2006;7:41–53. [PubMed: 16371949]

Alliot F, Rutin J, Leenen PJM, Pessac B. Pericytes and periendothelial cells of brain parenchyma vessels co-express aminopeptidase N, aminopeptidase A, and nestin. J Neurosci Res 1999;58:367–378. [PubMed: 10518110]

Alroy J, Goyal V, Skutelsky E. Lectin histochemistry of mammalian endothelium. Histochemistry 1987;86:603–607. [PubMed: 3610672]

Balding P, Gold ER. Observations on the reaction of en(a-)cells with sophora japonica haemagglutinin. Z Immunitatsforsch Exp Klin Immunol 1975;145:156–165. [PubMed: 126538]

Bao F, Dekaban GA, Weaver LC. Anti-CD11d antibody treatment reduces free radical formation and cell death in the injured spinal cord of rats. J Neurochem 2005;94:1361–1373. [PubMed: 15992367]

Bazzoni G, Dejana E. Endothelial cell-to-cell junctions: molecular organization and role in vascular homeostasis. Physiol Rev 2004;84:869–901. [PubMed: 15269339]

Belloni PN, Nicolson GL. Differential expression of cell surface glycoproteins on various organ-derived microvascular endothelia and endothelial cell cultures. J Cell Physiol 1988;136:398–410. [PubMed: 3170638]

Bolton SJ, Anthony DC, Perry VH. Loss of the tight junction proteins occludin and zonula occludens-1 from cerebral vascular endothelium during neutrophil-induced blood—brain barrier breakdown in vivo. Neuroscience 1998;86:1245–1257. [PubMed: 9697130]

Brabec RK, Peters BP, Bernstein IA, Gray RH, Goldstein IJ. Differential lectin binding to cellular membranes in the epidermis of the newborn rat. Proc Natl Acad Sci U S A 1980;77:477–479. [PubMed: 6928640]

Bullock R, Fujisawa H. The role of glutamate antagonists for the treatment of CNS injury. J Neurotrauma 1992;9(Suppl 2):S443–S462. [PubMed: 1613806]

Casella GT, Marcillo A, Bunge MB, Wood PM. New vascular tissue rapidly replaces neural parenchyma and vessels destroyed by a contusion injury to the rat spinal cord. Exp Neurol 2002;173:63–76. [PubMed: 11771939]

Casella GT, Bunge MB, Wood PM. Endothelial cell loss is not a major cause of neuronal and glial cell death following contusion injury of the spinal cord. Exp Neurol. 2006(in press)

Chan-Ling T, Page MP, Gardiner T, Baxter L, Rosinova E, Hughes S. Desmin ensheathment ratio as an indicator of vessel stability: evidence in normal development and in retinopathy of prematurity. Am J Pathol 2004;165:1301–1313. [PubMed: 15466395]

Chi L, Ke Y, Luo C, Gozal D, Liu R. Depletion of reduced glutathione enhances motor neuron degeneration in vitro and in vivo. Neuroscience 2007;144:991–1003. [PubMed: 17150307]

Debbage PL, Griebel J, Ried M, Gneiting T, DeVries A, Hutzler P. Lectin intravital perfusion studies in tumor-bearing mice: micrometer-resolution, wide-area mapping of microvascular labeling, distinguishing efficiently and inefficiently perfused microregions in the tumor. J Histochem Cytochem 1998;46:627–639. [PubMed: 9562571]

Dobrogowska DH, Vorbrodt AW. Immunogold localization of tight junctional proteins in normal and osmotically affected rat blood—brain barrier. J Mol Histol 2004;35:529–539. [PubMed: 15571330]

Edsbagge J, Johansson JK, Esni F, Luo Y, Radice GL, Semb H. Vascular function and sphingosine-1-phosphate regulate development of the dorsal pancreatic mesenchyme. Development 2005;132:1085–1092. [PubMed: 15689381]

Fatehi MI, Gerhart DZ, Myers TG, Drewes LR. Characterization of the blood—brain barrier: glycoconjugate receptors of 14 lectins in canine brain, cultured endothelial cells, and blotted membrane proteins. Brain Res 1987;415:30–39. [PubMed: 3304531]

Franz S, Frey B, Sheriff A, Gaipl US, Beer A, Voll RE, Kalden JR, Herrmann M. Lectins detect changes of the glycosylation status of plasma membrane constituents during late apoptosis. Cytometry 2006;A69:230–239. [PubMed: 16498674]

Fujiki M, Zhang Z, Guth L, Steward O. Genetic influences on cellular reactions to spinal cord injury: activation of macrophages/microglia and astrocytes is delayed in mice carrying a mutation (WldS) that causes delayed Wallerian degeneration. J Comp Neurol 1996;371:469–484. [PubMed: 8842900]

Galili U, Shohet SB, Kobrin E, Stults CL, Macher BA. Man, apes, and Old World monkeys differ from other mammals in the expression of alpha-galactosyl epitopes on nucleated cells. J Biol Chem 1988;263:17755–17762. [PubMed: 2460463]

Ge S, Pachter JS. Isolation and culture of microvascular endothelial cells from murine spinal cord. J Neuroimmunol 2006;177:209–214. [PubMed: 16806499]

Glaser J, Gonzalez R, Perreau VM, Cotman CW, Keirstead HS. Neutralization of the chemokine CXCL10 enhances tissue sparing and angiogenesis following spinal cord injury. J Neurosci Res 2004;77:701–708. [PubMed: 15352216]

Gris D, Marsh DR, Oatway MA, Chen Y, Hamilton EF, Dekaban GA, Weaver LC. Transient blockade of the CD11d/CD18 integrin reduces secondary damage after spinal cord injury, improving sensory, autonomic, and motor function. J Neurosci 2004;24:4043–4051. [PubMed: 15102919]

Hamm S, Dehouck B, Kraus J, Wolburg-Buchholz K, Wolburg H, Risau W, Cecchelli R, Engelhardt B, Dehouck MP. Astrocyte mediated modulation of blood—brain barrier permeability does not correlate with a loss of tight junction proteins from the cellular contacts. Cell Tissue Res 2004;315:157–166. [PubMed: 14615934]

Han HS, Suk K. The function and integrity of the neurovascular unit rests upon the integration of the vascular and inflammatory cell systems. Curr Neurovasc Res 2005;2:409–423. [PubMed: 16375722]

Hayes CE, Goldstein IJ. An alpha-D-galactosyl-binding lectin from Bandeiraea simplicifolia seeds. Isolation by affinity chromatography and characterization. J Biol Chem 1974;249:1904–1914. [PubMed: 4206402]

Hirasawa T, Ohsawa K, Imai Y, Ondo Y, Akazawa C, Uchino S, Kohsaka S. Visualization of microglia in living tissues using Iba1-EGFP transgenic mice. J Neurosci Res 2005;81:357–362. [PubMed: 15948177]

Hsu CJ, McKeon R, Goussev S, Werb Z, Lee J, Trivedi A, Noble-Haeusslein LJ. Matrix metalloproteinase-2 facilitates wound healing events that promote functional recovery after spinal cord injury. J Neurosci 2006;26:9841–9850. [PubMed: 17005848]

Hughes S, Chang-Ling T. Roles of endothelial cell migration and apoptosis in vascular remodeling during development of the central nervous system. Microcirculation 2000;7:317–333. [PubMed: 11079250]

Hughes S, Gardiner T, Hu P, Baxter L, Rosinova E, Chan-Ling T. Altered pericyte—endothelial relations in the rat retina during aging: implications for vessel stability. Neurobiol Aging 2006;27:1838–1847. [PubMed: 16387390]

Iruela-Arispe ML, Rodriguez-Manzaneque JC, bu-Jawdeh G. Endo-metrial endothelial cells express estrogen and progesterone receptors and exhibit a tissue specific response to angiogenic growth factors. Microcirculation 1999;6:127–140. [PubMed: 10466115]

Jaeger CB, Blight AR. Spinal cord compression injury in guinea pigs: structural changes of endothelium and its perivascular cell associations after blood—brain barrier breakdown and repair. Exp Neurol 1997;144:381–399. [PubMed: 9168838]

Jakovcevski I, Wu J, Karl N, Leshchyns'ka I, Sytnyk V, Chen J, Irintchev A, Schachner M. Glial scar expression of CHL1, the close homolog of the adhesion molecule L1, limits recovery after spinal cord injury. J Neurosci 2007;27:7222–7233. [PubMed: 17611275]

Jilani SM, Murphy TJ, Thai SN, Eichmann A, Alva JA, Iruela-Arispe ML. Selective binding of lectins to embryonic chicken vasculature. J Histochem Cytochem 2003;51:597–604. [PubMed: 12704207]

Kigerl KA, McGaughy VM, Popovich PG. Comparative analysis of lesion development and intraspinal inflammation in four strains of mice following spinal contusion injury. J Comp Neurol 2006;494:578–594. [PubMed: 16374800]

Kokovay E, Li L, Cunningham LA. Angiogenic recruitment of pericytes from bone marrow after stroke. J Cereb Blood Flow Metab 2006;26:545–555. [PubMed: 16121128]

Koyanagi I, Tator CH, Lea PJ. Three-dimensional analysis of the vascular system in the rat spinal cord with scanning electron microscopy of vascular corrosion casts. Part 2: acute spinal cord injury. Neurosurgery 1993;33:285–291. [PubMed: 8367052]

Laitinen L. *Griffonia simplicifolia* lectins bind specifically to endothelial cells and some epithelial cells in mouse tissues. Histochem J 1987;19:225–234. [PubMed: 3597137]

Lippoldt A, Kniesel U, Liebner S, Kalbacher H, Kirsch T, Wolburg H, Haller H. Structural alterations of tight junctions are associated with loss of polarity in stroke-prone spontaneously hypertensive rat blood—brain barrier endothelial cells. Brain Res 2000;885:251–261. [PubMed: 11102579]

Lowe JB. Glycan-dependent leukocyte adhesion and recruitment in inflammation. Curr Opin Cell Biol 2003;15:531–538. [PubMed: 14519387]

Loy DN, Crawford CH, Darnall JB, Burke DA, Onifer SM, Whittemore SR. Temporal progression of angiogenesis and basal lamina deposition after contusive spinal cord injury in the adult rat. J Comp Neurol 2002;445:308–324. [PubMed: 11920709]

Ma M, Basso DM, Walters P, Stokes BT, Jakeman LB. Behavioral and histological outcomes following graded spinal cord contusion injury in the C57Bl/6 mouse. Exp Neurol 2001;169:239–254. [PubMed: 11358439]

Mark KS, Davis TP. Cerebral microvascular changes in permeability and tight junctions induced by hypoxia-reoxygenation. Am J Physiol Heart Circ Physiol 2002;282:H1485–H1494. [PubMed: 11893586]

Mautes AE, Weinzierl MR, Donovan F, Noble LJ. Vascular events after spinal cord injury: contribution to secondary pathogenesis. Phys Ther 2000;80:673–687. [PubMed: 10869130]

Mazzetti S, Frigerio S, Gelati M, Salmaggi A, Vitellaro-Zuccarello L. *Lycopersicon esculentum* lectin: an effective and versatile endothelial marker of normal and tumoral blood vessels in the central nervous system. Eur J Histochem 2004;48:423–428. [PubMed: 15718209]

McEwen BS, Reagan LP. Glucose transporter expression in the central nervous system: relationship to synaptic function. Eur J Pharmacol 2004;490:13–24. [PubMed: 15094070]

Morgenstern DA, Asher RA, Fawcett JW. Chondroitin sulphate proteoglycans in the CNS injury response. Prog Brain Res 2002;137:313–332. [PubMed: 12440375]

Morioka T, Kalehua AN, Streit WJ. Characterization of microglial reaction after middle cerebral artery occlusion in rat brain. J Comp Neurol 1993;327:123–132. [PubMed: 8432904]

Nag S. Cerebral endothelial surface charge in hypertension. Acta Neuropathol 1984;63:276–281. [PubMed: 6475487]

Nico B, Quondamatteo F, Ribatti D, Bertossi M, Russo G, Herken R, Roncali L. Ultrastructural localization of lectin binding sites in the developing brain microvasculature. Anat Embryol 1998;197:305–315. [PubMed: 9565323]

Nico B, Quondamatteo F, Herken R, Blumchen T, Defazio G, Giorelli M, Livrea P, Marzullo A, Russo G, Ribatti D, Roncali L. Interferon beta-1a prevents the effects of lipopolysaccharide on embryonic brain microvessels. Brain Res Dev Brain Res 2000;119:231–242.

Niethammer AG, Xiang R, Becker JC, Wodrich H, Pertl U, Karsten G, Eliceiri BP, Reisfeld RA. A DNA vaccine against VEGF receptor 2 prevents effective angiogenesis and inhibits tumor growth. Nat Med 2002;8:1369–1375. [PubMed: 12415261]

Nishida S, Akai F, Hiruma S, Maeda M, Tanji K, Hashimoto S. Experimental study of WGA binding on the endothelial cell surface in cerebral ischemia. Histol Histopathol 1986;1:69–74. [PubMed: 2980103]

Nitta T, Masaki H, Gotoh S, Seo Y, Sasaki H, Hashimoto N, Furuse M, Tsukita S. Size-selective loosening of the blood—brain barrier in claudin-5-deficient mice. J Cell Biol 2003;161:653–660. [PubMed: 12743111]

Noble LJ, Wrathall JR. Spinal cord contusion in the rat: morphometric analyses of alterations in the spinal cord. Exp Neurol 1985;88:135–149. [PubMed: 3979507]

Noble LJ, Wrathall JR. Correlative analyses of lesion development and functional status after graded spinal cord contusive injuries in the rat. Exp Neurol 1989a;103:34–40. [PubMed: 2912748]

Noble LJ, Wrathall JR. Distribution and time course of protein extravasation in the rat spinal cord after contusive injury. Brain Res 1989b;482:57–66. [PubMed: 2706482]

Noble LJ, Mautes AE, Hall JJ. Characterization of the microvascular glycocalyx in normal and injured spinal cord in the rat. J Comp Neurol 1996;376:542–556. [PubMed: 8978469]

Noguera-Troise I, Daly C, Papadopoulos NJ, Coetzee S, Boland P, Gale NW, Lin HC, Yancopoulos GD, Thurston G. Blockade of Dll4 inhibits tumour growth by promoting non-productive angiogenesis. Nature 2006;444:1032–1037. [PubMed: 17183313]

Nourhaghighi N, Teichert-Kuliszewska K, Davis J, Stewart DJ, Nag S. Altered expression of angiopoietins during blood—brain barrier breakdown and angiogenesis. Lab Invest 2003;83:1211–1222. [PubMed: 12920250]

Oatway MA, Chen Y, Bruce JC, Dekaban GA, Weaver LC. Anti-CD11d integrin antibody treatment restores normal serotonergic projections to the dorsal, intermediate, and ventral horns of the injured spinal cord. J Neurosci 2005;25:637–647. [PubMed: 15659600]

Papaioannou VE, Fox JG. Efficacy of tribromoethanol anesthesia in mice. Lab Anim Sci 1993;43:189–192. [PubMed: 8320967]

Pardridge WM. Transport of insulin-related peptides and glucose across the blood—brain barrier. Ann N Y Acad Sci 1993;692:126–137. [PubMed: 8215017]

Pardridge WM. Blood—brain barrier delivery. Drug Discov Today 2007;12:54–61. [PubMed: 17198973]

Perdiki M, Farooque M, Holtz A, Li GL, Olsson Y. Expression of endothelial barrier antigen immunoreactivity in blood vessels following compression trauma to rat spinal cord. Temporal evolution and relation to the degree of the impact. Acta Neuropathol 1998;96:8–12. [PubMed: 9678508]

Peters BP, Goldstein IJ. The use of fluorescein-conjugated *Bandeiraea simplicifolia* B4-isolectin as a histochemical reagent for the detection of alpha-D-galactopyranosyl groups. Their occurrence in basement membranes. Exp Cell Res 1979;120:321–334. [PubMed: 436961]

Ponder BA, Wilkinson MM. Organ-related differences in binding of *Dolichos biflorus* agglutinin to vascular endothelium. Dev Biol 1983;96:535–541. [PubMed: 6832482]

Popovich PG, Wei P, Stokes BT. Cellular inflammatory response after spinal cord injury in Sprague-Dawley and Lewis rats. J Comp Neurol 1997;377:443–464. [PubMed: 8989657]

Porter GA, Palade GE, Milici AJ. Differential binding of the lectins *Griffonia simplicifolia* I and *Lycopersicon esculentum* to microvascular endothelium: organ-specific localization and partial glycoprotein characterization. Eur J Cell Biol 1990;51:85–95. [PubMed: 2328740]

Raub TJ. Signal transduction and glial cell modulation of cultured brain microvessel endothelial cell tight junctions. Am J Physiol 1996;271:C495–C503. [PubMed: 8769988]

Richter MW, Fletcher PA, Liu J, Tetzlaff W, Roskams AJ. Lamina propria and olfactory bulb ensheathing cells exhibit differential integration and migration and promote differential axon sprouting in the lesioned spinal cord. J Neurosci 2005;25:10700–10711. [PubMed: 16291943]

Sennino B, Falcón BL, McAuley D, Le T, McCauley T, Kurz JC, Haskell A, Epstein DM, McDonald DM. Sequential loss of tumor vessel pericytes and endothelial cells after inhibition of platelet-derived growth factor B by selective aptamer AX102. Cancer Res 2007;67:7358–7367. [PubMed: 17671206]

Stamatovic SM, Shakui P, Keep RF, Moore BB, Kunkel SL, Van Rooijen N, Andjelkovic AV. Monocyte chemoattractant protein-1 regulation of blood—brain barrier permeability. J Cerebral Blood Flow Metab 2005;25:593–606.

Streit WJ, Schulte BA, Balentine DJ, Spicer SS. Histochemical localization of galactose-containing glycoconjugates in sensory neurons and their processes in the central and peripheral nervous system of the rat. J Histochem Cytochem 1985;33:1042–1052. [PubMed: 4045182]

Thurston G, Baluk P, Hirata A, McDonald DM. Permeability-related changes revealed at endothelial cell borders in inflamed venules by lectin binding. Am J Physiol 1996;271:H2547–H2562. [PubMed: 8997316]

Vinores SA, Derevjanik NL, Vinores MA, Okamoto N, Campochiaro PA. Sensitivity of different vascular beds in the eye to neovascularization and blood—retinal barrier breakdown in VEGF transgenic mice. Adv Exp Med Biol 2000;476:129–138. [PubMed: 10949661]

Vinores SA, Seo MS, Derevjanik NL, Campochiaro PA. Photoreceptor-specific overexpression of platelet-derived growth factor induces proliferation of endothelial cells, pericytes, and glial cells and aberrant vascular development: an ultrastructural and immunocytochemical study. Brain Res Dev Brain Res 2003;140:169–183.

Vischer UM. von Willebrand factor, endothelial dysfunction, and cardiovascular disease. J Thromb Haemost 2006;4:1186–1193. [PubMed: 16706957]

Vorbrodt AW. Changes in the distribution of endothelial surface glycoconjugates associated with altered permeability of brain microblood vessels. Acta Neuropathol 1986;70:103–111. [PubMed: 3739620]

Vorbrodt AW, Dobrogowska DH. Molecular anatomy of intercellular junctions in brain endothelial and epithelial barriers: electron microscopist's view. Brain Res Brain Res Rev 2003;42:221–242. [PubMed: 12791441]

Vorbrodt AW, Lossinsky AS, Dobrogowska DH, Wisniewski HM. Distribution of anionic sites and glycoconjugates on the endothelial surfaces of the developing blood—brain barrier. Brain Res 1986;394:69–79. [PubMed: 3756533]

Vorbrodt AW, Dobrogowska DH, Tarnawski M. Immunogold study of interendothelial junction-associated and glucose transporter proteins during postnatal maturation of the mouse blood—brain barrier. J Neurocytol 2001;30:705–716. [PubMed: 12118158]

Whetstone WD, Hsu JY, Eisenberg M, Werb Z, Noble-Haeusslein LJ. Blood—spinal cord barrier after spinal cord injury: relation to revascularization and wound healing. J Neurosci Res 2003;74:227–239. [PubMed: 14515352]

Willis CL, Leach L, Clarke GJ, Nolan CC, Ray DE. Reversible disruption of tight junction complexes in the rat blood—brain barrier, following transitory focal astrocyte loss. Glia 2004;48:1–13. [PubMed: 15326610]

Wolburg H, Wolburg-Buchholz K, Kraus J, Rascher-Eggstein G, Liebner S, Hamm S, Duffner F, Grote EH, Risau W, Engelhardt B. Localization of claudin-3 in tight junctions of the blood—brain barrier is selectively lost during experimental autoimmune encephalomyelitis and human glioblastoma multiforme. Acta Neuropathol 2003;105:586–592. [PubMed: 12734665]

Wu CH, Wen CY, Shieh JY, Ling EA. Remodeling of membrane-bound glycoproteins containing alpha-D-galactose in the cerebral endothelial cells of rats during blood—brain barrier maturation and alteration. J Hirnforsch 1997;38:541–552. [PubMed: 9476218]

Yamauchi T, Lin Y, Sharp FR, Noble-Haeusslein LJ. Hemin induces heme oxygenase-1 in spinal cord vasculature and attenuates barrier disruption and neutrophil infiltration in the injured murine spinal cord. J Neurotrauma 2004;21:1017–1030. [PubMed: 15319001]
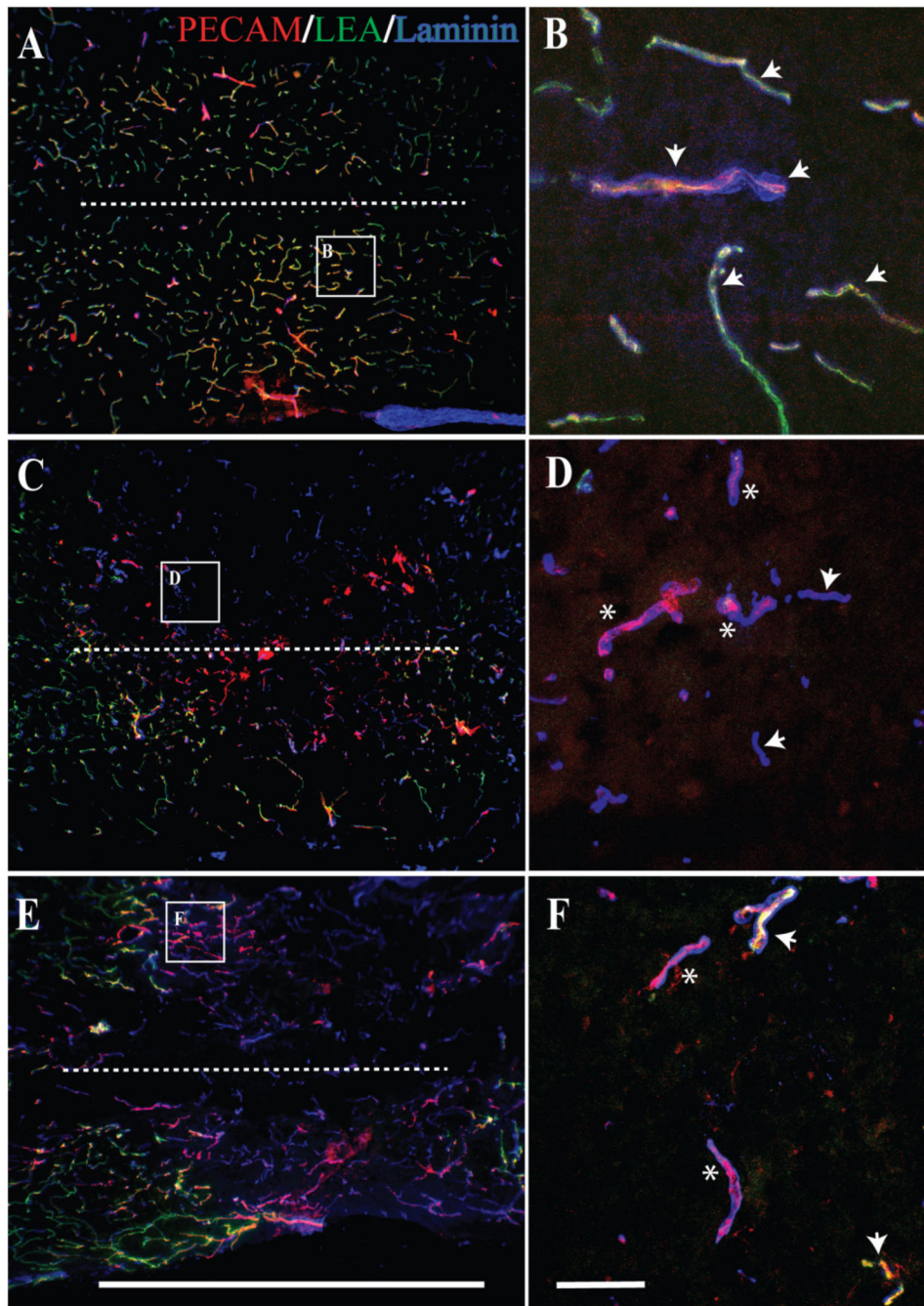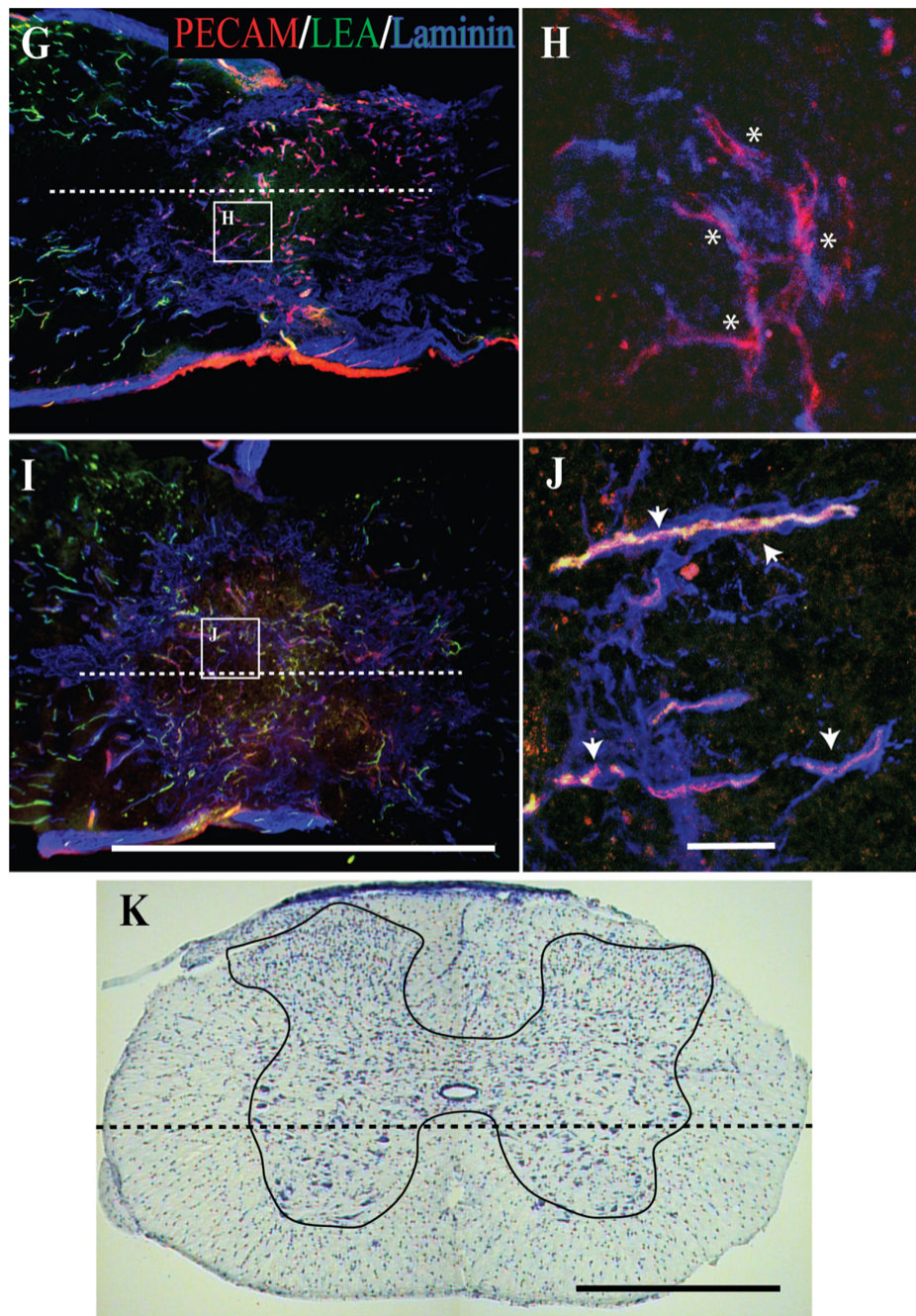
Fig. 1.
(Overleaf). Analysis of vascularity and microvascular perfusion at the epicenter of the injured adult mouse spinal cord 1, 3, 7, and 14 days post-SCI demonstrates a differential microvascular phenotype. To determine this, longitudinal sections of injury epicenters were examined and compared with tissue from normal controls. In the normal mouse spinal cord, a dense microvascular network is apparent (**A**,**B**, arrowheads), exhibiting normal anatomy including a continuous basal lamina (AMCA-laminin-ir), an intact endothelium (TRITC-PECAM-1-ir), and luminal LEA glycocalyx binding of perfused vessels (FITC-LEA). By 1 day post-SCI, a hypovascularity of the SCI epicenter is readily observed (**C**). Most important is that differential microvascular phenotypes are apparent, including nonperfused vascular elements exhibiting

both an intact (**D**; asterisks) and an absent (D; arrowheads) endothelium. At 3 days following SCI (**E**), most of the vascular profiles within the epicenter exhibit an intact endothelium (**F**; asterisks), with some observed perfusion (F; arrowheads). Seven days following SCI, a significant amount of extravascular laminin is apparent within the injury epicenter (**G**). In the high-magnification inset (**H**), vascular profiles can be observed containing a more robust endothelium (H; asterisks). Importantly, not until 14 days post-SCI (**I**) do most microvascular profiles in the injury epicenter exhibit a significant restoration of their perfusion state (**J**; arrowheads). The dashed line in the cresyl violet-stained cross-section of mouse spinal cord (**K**; gray matter is traced) illustrates the approximate longitudinal plane of sections represented in A—J. The midline of longitudinal sections is approximated by the dashed lines in A,C,E,G,I. Scale bars = 1 mm in E (applies to A,C,E); 1 mm in I (applies to G,I); 1 mm in K; 20 μm in F (applies to B,D,F); 20 μm in J (applies to H,J).
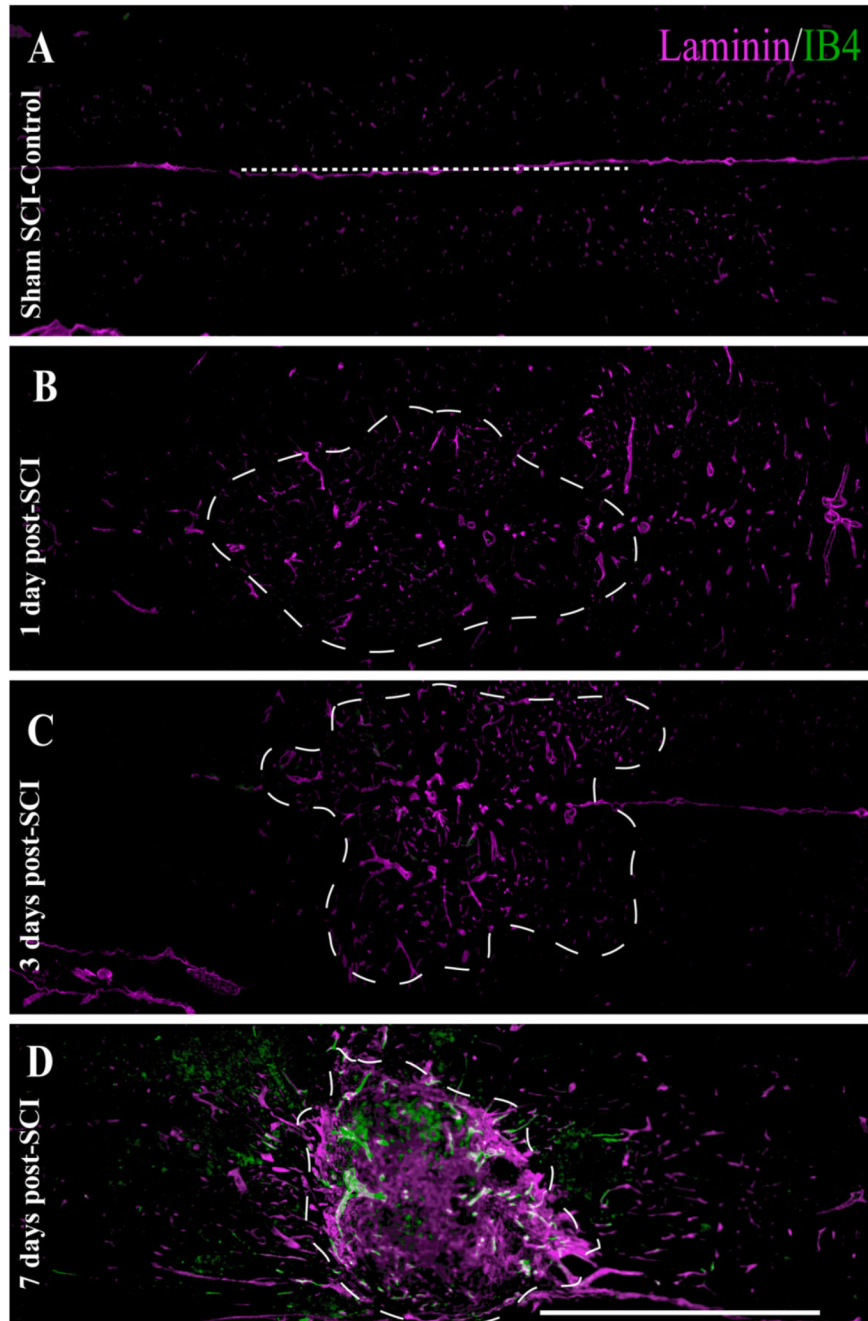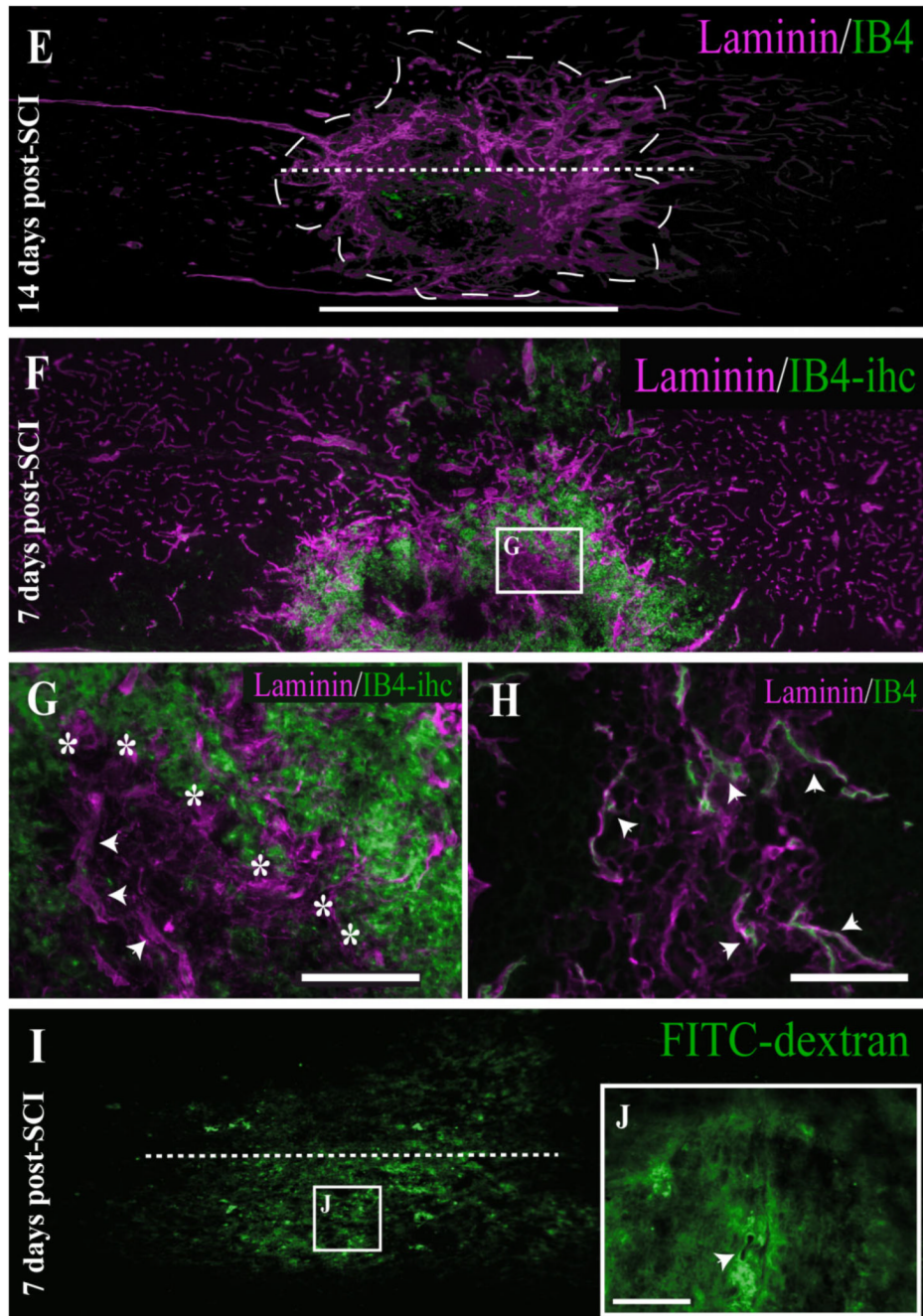
Fig. 2.
(Overleaf). Both temporal and spatial analysis of angiogenic microvessels at the injury epicenter shows maximal binding of IB4 7 days following SCI. In control spinal tissue (**A**), laminin immunoreactivity (ir) is limited to the basal lamina of the vasculature, with no IB4 vascular binding observed. By 1 day post-SCI (**B**), no significant IB4 binding is observed in the evolving injury epicenter (hatched outline) despite slightly enlarged laminin-ir vascular profiles, which is an indication of microvascular activation. By 3 days following SCI (**C**), this vascular activation is more apparent, with more enlarged vascular profiles obvious within the evolving epicenter. By 7 days following injury (**D**), IB4-bound spinal vessels within the injury epicenter are overtly present, which is characteristic of the evolving murine SCI. By 14 days

post-SCI (**E**), qualitative expression of the IB4 vascular phenotype is dramatically decreased at the injury epicenter. The vascular IB4 binding obtained via intravascular application is quite different from that obtained by histochemical application to 7-day injured spinal cord tissue (**F,G**) in that the majority of IB4 staining is observed in inflammatory cells (G; boundary indicated by asterisks) with little associated with laminin-immunopositive vascular profiles (G; arrowheads). This is in contrast to the resolution of microvascular elements observed within the injury epicenter achieved by intravascular administration (**H**, arrowheads). The IB4 binding is specific, in that intravital application of molecular-weight-matched FITC-dextran 7 days post-SCI results in diffuse signal within the injury epicenter (**I,J**), indicative of overt microvascular permeability that is apparent in the perivascular tissue surrounding a small vessel (J, arrowhead). As in Figure 1, the midline of longitudinal sections is approximated by the dashed lines in A,E,I, which is consistent with the other unlabeled longitudinal fields presented. Scale bars = 1 mm in D (applies to A—D); 1 mm in E (applies to E,F,I); 1 mm in K; 20 μm in F (applies to B,D,F); 20 μm in J (applies to H,I); 100 μm in G,H,J.

A   PECAM Immunostaining

B   Intravascular LEA Binding

C   Intravascular IB4 Binding
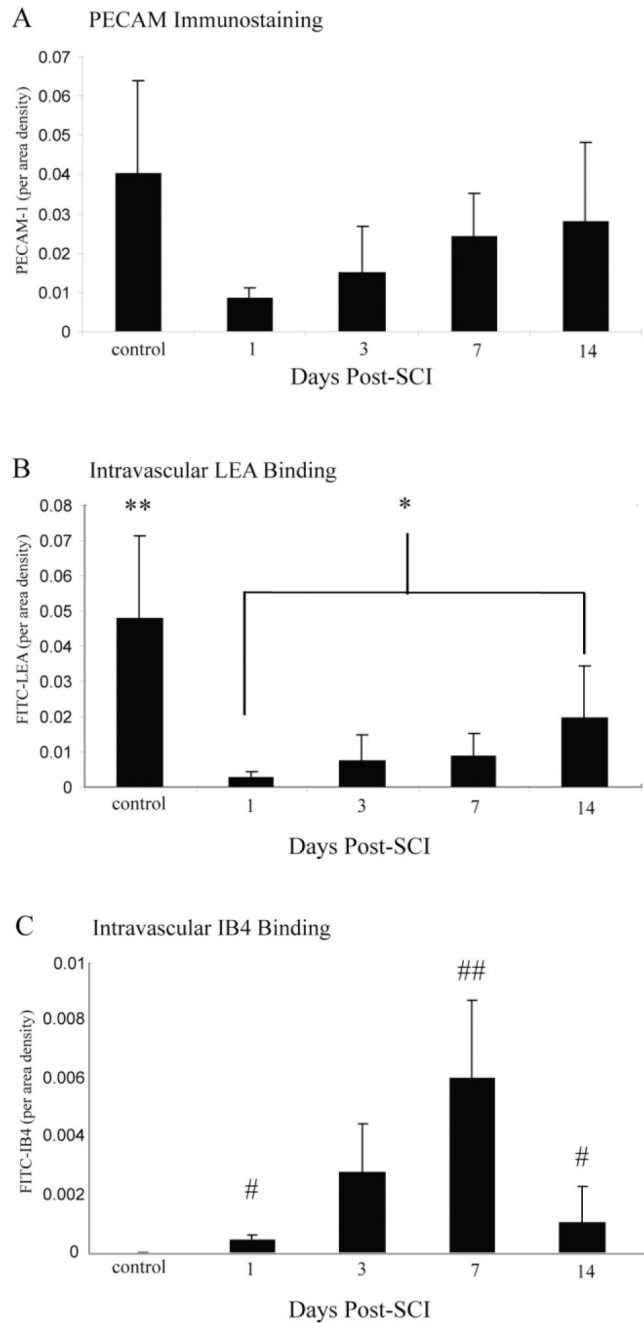
Fig. 3.
By comparing the quantitative temporal representation of LEA/IB4/PECAM-1 in the injury epicenter, a clearer understanding of microvascular plasticity associated with the evolution of the secondary injury cascade is apparent. Total vascularity of the injury epicenter was assessed by PECAM-1 immunoreactivity (**A**) and was found to be dramatically decreased by 24 hours following SCI, with levels increasing consistently through 2 weeks following injury. The perfusion status of spinal microvessels at the injury epicenter was assessed by intravascular LEA lectin binding (**B**). Perfusion of the injury epicenter is significantly decreased by 1 day following SCI concomitant with the acute phase of vascular regression. Spinal perfusion status does not rebound in lock step with revascularization, because levels of LEA bound vascular

profiles are not significantly greater than those observed in the 24 hour post-SCI time point until 14 days postinjury. The appearance of the IB4-bound vascular phenotype is tightly temporally regulated (**C**), with significant numbers of profiles (relative to controls) first observed 1 day following SCI. Numbers of IB4-bound spinal vessels in the injury epicenter reach maximal levels 1 week following injury and decline by 2 weeks following SCI, with numbers approaching baseline by 4 weeks post-SCI (data not shown). Quantitative data represent the per area density of PECAM-1-ir, intravascular LEA, and intravascular IB4 labeling/injury epicenter $\pm$ SD. Levels are significant as determined by one-way ANOVA results and Tukey HSD post hoc *t*-tests. **Vascular LEA binding is significantly greater in controls ($P < 0.001$, df = 4,16, F = 20.275) relative to all experimental groups. *Vascular LEA binding is significantly greater ($P < 0.05$, df = 4,16, F = 20.275) than 1 day post-SCI. [#]Vascular IB4 binding is significantly greater than controls ($P < 0.05$, df = 3,12, F = 8.6). [##]Vascular IB4 binding is significantly greater ($P < 0.01$, df = 3,12, F = 8.6) than all experimental groups.
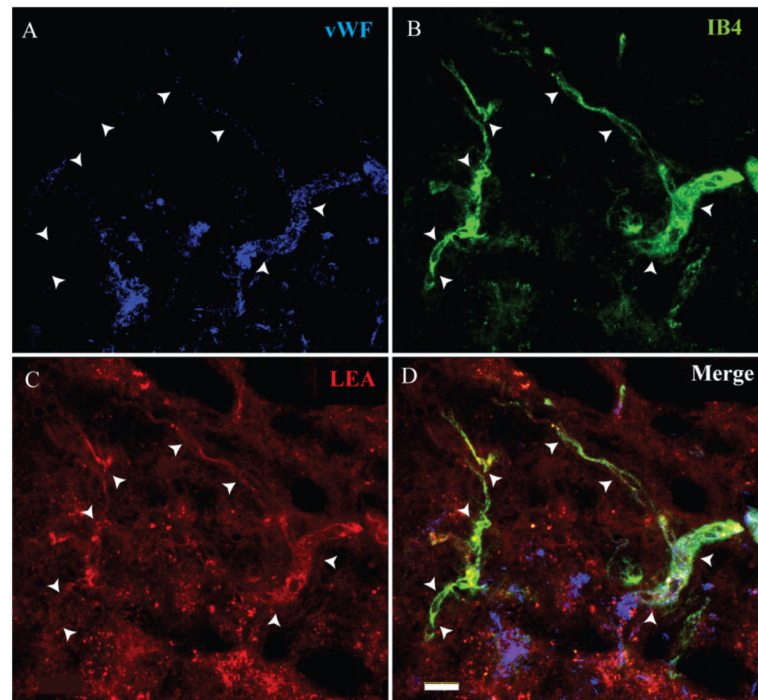
Fig. 4.
FITC-IB4-bound microvessels are shown within the injury epicenter 7 following SCI (**B**). IB4-labeled microvessels within the injury epicenter are confirmed by vWF immunoreactivity (**A**). These vascular profiles are observed to be perfused as demonstrated by intraluminal staining with TRITC-LEA (**C**). The merged image (**D**) identifies a representative microvascular profile (arrowheads) observed to colabel with both intravascular tracers. Scale bar = 20 μm.
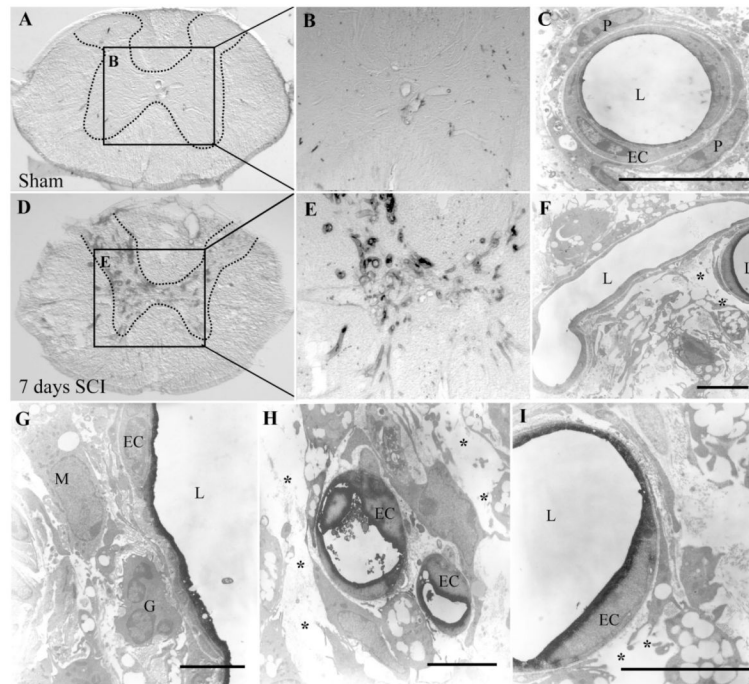
Fig. 5.
In control spinal cord sections (**A**—**C**), immuno-EM staining for IB4 shows no binding of the lectin in spinal microvessels neither within spinal gray (hatched outline) nor white matter. In contrast, in spinal tissue taken 7 days post-SCI (**D,E**), many IB4-bound microvascular profiles are seen, especially within injured spinal gray matter (hatched outline). Higher magnification micrographs show the normal ultrastructure of spinal capillaries (C), with endothelial cells (EC) immediately invested by pericytes (P). In injured spinal tissue, this ultrastructure is pathologically altered, with IB4-bound microvessels demonstrating a lack of obvious pericytic investment (**F**—**I**) and significant disruption of abluminal matrix (F,H,I, asterisks). Furthermore, many IB4-bound microvessels are observed to be in close association with inflammatory cells (G,H), including putative macrophages (M) and granulocytes (G) with a single endothelial profile present with its associated vascular lumen (L). Scale bars = 5 μm.
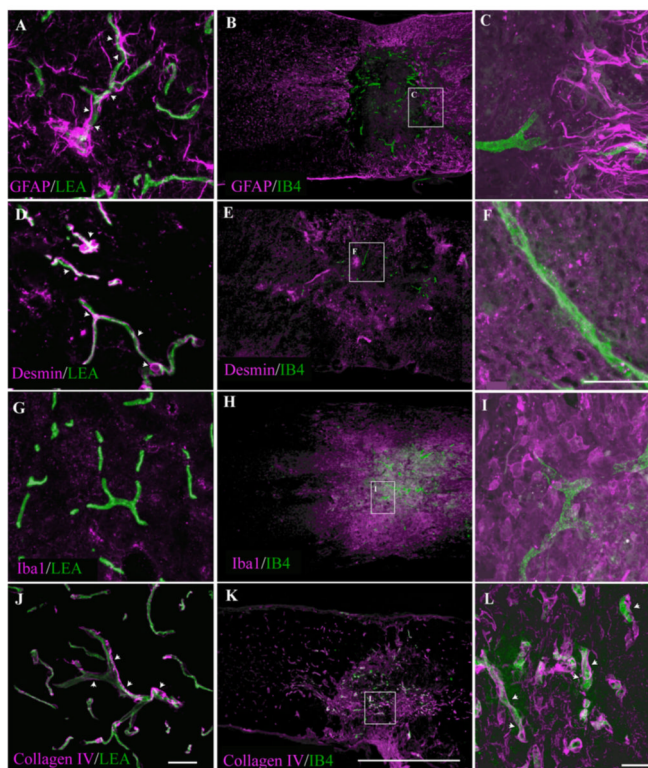
Fig. 6.
Immunohistochemical characterization of epicenter microenvironment 7 days post-SCI demonstrates significant histopathology concomitant with IB4 microvascular binding. Normal association of astrocytes (**A**) and pericytes (**D**) with spinal microvessels is shown in control tissue as demonstrated by GFAP and desmin immunoreactivity, respectively. At 7 days post-SCI, there is a loss of both vascular-associated GFAP (**B,C**) and desmin immunoreactivity (**E,F**) at the epicenter, indicating disruption of astrocytic perivascular endfeet and pericytic investment, respectively. Also, no overt inflammation is observed in control spinal tissue as demonstrated by a lack of Iba1 immunoreactivity (**G**). In injured spinal tissue, a significant inflammation is associated with epicenter vascular activation as demonstrated by association of IB4 and Iba1 immunoreactivity (**H,I**). Seven days following SCI, both IB4-bound and IB4-unbound microvessels demonstrate associated collagen IV immunoreactivity within the evolving lesion epicenter (**K,L**, arrowheads), suggesting a preservation of nonpathological basal lamina phenotype comparable to that observed with microvascular profiles in control tissue (**J**, arrowheads). Scale bars = 20 μm in J (applies to A,D,G,J); 20 μm in F (applies to C,F,I); 1 mm in K (applies to B,E,H,K); 20 μm in L.
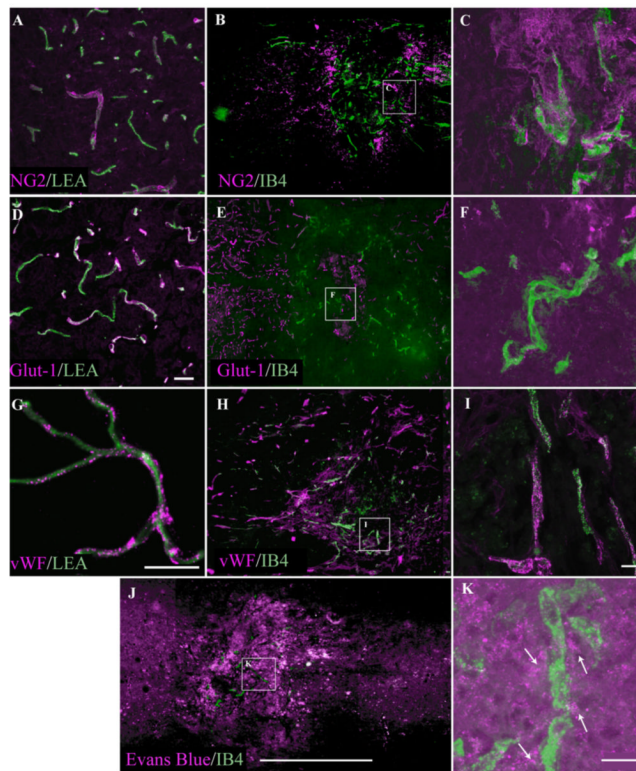
Fig. 7.
Alteration of spinal microvascular phenotype exemplifies pathological alteration and loss of microvascular function. At 7 days post-SCI, IB4-bound vessels exhibit high levels of immunoreactivity for the proteoglycan NG2 (**B,C**), demonstrating EC activation not observed in microvessels in control spinal tissue (**A**). Conversely, IB4-bound microvessels demonstrate a loss of Glut-1 immunoreativity (**E,F**), which is characteristic of normal spinal vessels (**D**) and demonstrates loss of normal metabolic capacity, an important spinal microvascular function. Normal spinal microvessels express von Willebrand factor (**G**), which is preserved in IB4-bound spinal microvessels (**H,I**). Most importantly is that significant extravasation of Evans blue is seen associated with the IB4 vascular phenotype (**J,K**, arrows), demonstrating that IB4-reactive microvessels are leaky. Scale bars = 20 μm in D (applies to A,D); 20 μm in G; 20 μm in I (applies to C,F,I); 20 μm in K; 1 mm in J (applies to B,E,H,J).
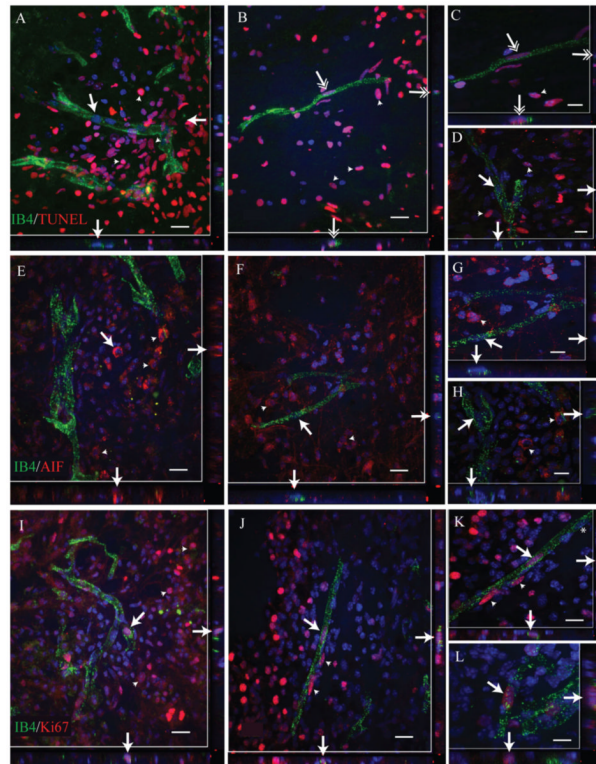
Fig. 8.
Comparison of nuclear markers of cell death and proliferation in endothelial cells of IB4-positive spinal microvessels demonstrates population of proliferative phenotypes. In spinal microvessels at the injury epicenter 7 days following SCI, IB4 vascular endothelial cells appear largely TUNEL immunonegative (**A,D**, single-tipped arrows; arrowheads indicate positive nonvascular cells). In some cases, endothelial cells associated with IB4-bound microvessels appear to be TUNEL immunopositive (**B,C**; double-tipped arrows; arrowheads delineate positive nonvascular cells), although associated nuclear condensation or fragmentation, typical for apoptotic cells, was not observed. Similarly, no AIF-immunopositive endothelial cells are observed (**E—H**, arrows) despite the presence of AIF-immunopositive nonvascular cells seen in the fields (arrowheads). By relative comparison with both TUNEL- and AIF-immunnopositive endothelial cells, many more IB4-bound endothelial cells appear to be proliferative as indicated by their expression of Ki67 immnuopositivity (**I—L**, arrows). In some cases, several endothelial cell nuclei associated with a single IB4 microvascular profile are Ki67 immnuopositive (K, arrows/arrowheads), with clearly Ki67-immunonegative EC nuclei also evident (K, asterisk). Scale bars = 20 μm in A,B,E,F,I,J; 10 μm in C,D,G,H,K,L.
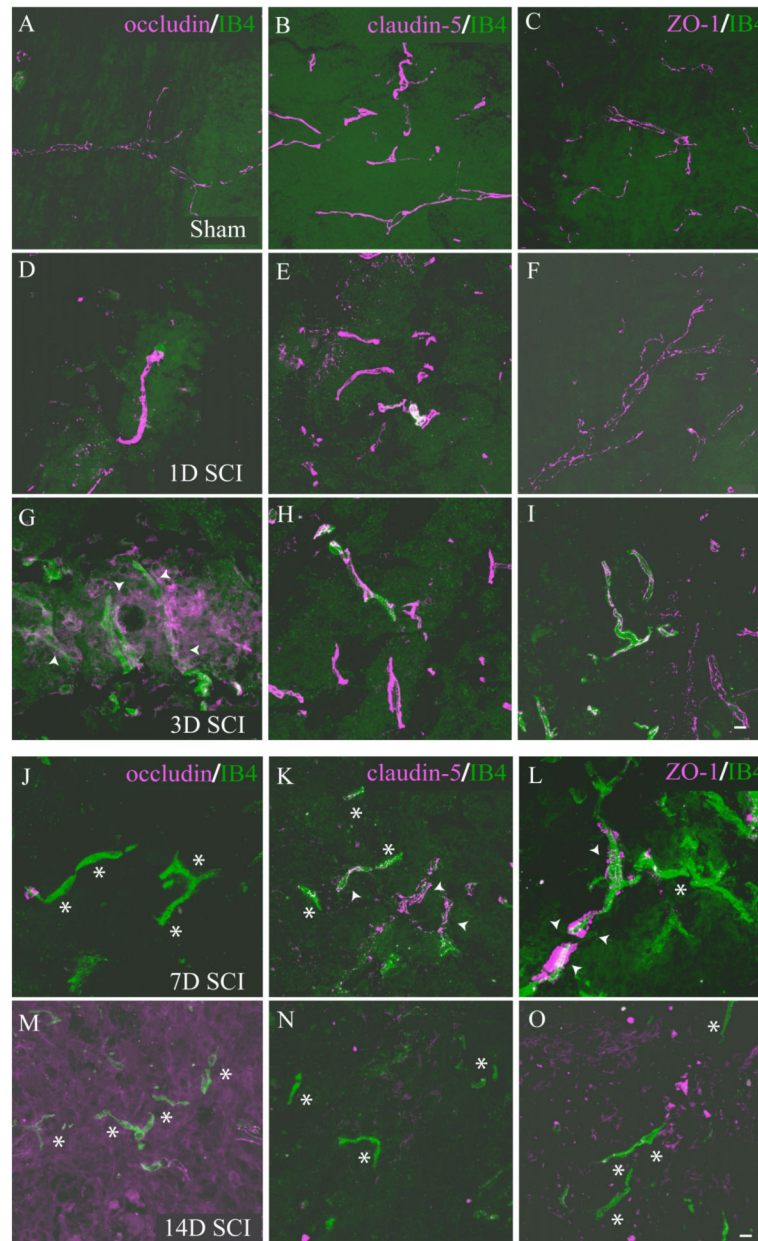
Fig. 9.
IB4-bound endothelial cells demonstrate pathological basal tight junction (TJ) phenotype 7 days following SCI. In control spinal tissue, endothelial cells of normal microvessels express the TJ proteins occludin (**A**), claudin-5 (**B**), and ZO-1 (**C**). This normal endothelial staining pattern is largely maintained in microvessels 1 day post-SCI (**D—F**), with only occludin (**G**) exhibiting initial pathological immunostaining at 3 days post-SCI, with other TJ components remaining unaffected (**H,I**). By contrast, at 7 days following injury (J), IB4-bound microvessels express pathological patterns of the apical TJ component claudin-5 (**K**, arrowheads) and ZO-1 (**L**, arrowheads) but do not express the basal TJ component occludin (**N**, asterisks), although some IB4 profiles are observed in these fields that do not overtly express any of the TJ markers examined (K,L; asterisks). At 14 days postinjury, IB4-bound microvessels express neither basal (**M**) nor apical (**N,O**) TJ components, demonstrating destabilization of microvascular

integrity in the injured spinal cord. Scale bars = 10 μm in I (applies to A—I); 10 μm in O (applies to J—O).